ORIGINAL ARTICLE

PMS2 variant results in loss of ATPase activity without compromising mismatch repair

Brandon M. D'Arcy[1,2] | Jennifer Arrington[1,2] | Justin Weisman[1,2] | Steven B. McClellan[1,3] | Vandana[1,2] | Zhengrong Yang[4] | Champion Deivanayagam[4] | Jessa Blount[5] | Aishwarya Prakash[1,2]

[1]Mitchell Cancer Institute, University of South Alabama Health, Mobile, Alabama, USA

[2]Department of Biochemistry and Molecular Biology, University of South Alabama, Mobile, Alabama, USA

[3]Flow Cytometry Shared Resource Lab, Mitchell Cancer Institute, Mobile, Alabama, USA

[4]Department of Biochemistry and Molecular Genetics, School of Medicine University of Alabama at Birmingham, Birmingham, Alabama, USA

[5]Circulogene Theranostics, Birmingham, Alabama, USA

Correspondence
Aishwarya Prakash, Mitchell Cancer Institute, University of South Alabama Health, 1660 Springhill Avenue, Mobile, AL 36604, USA.
Email: aprakash@southalabama.edu

Abstract

Hereditary cancer syndromes account for approximately 5%–10% of all diagnosed cancer cases. Lynch syndrome (LS) is an autosomal dominant hereditary cancer condition that predisposes individuals to an elevated lifetime risk for developing colorectal, endometrial, and other cancers. LS results from a pathogenic mutation in one of four mismatch repair (MMR) genes (*MSH2*, *MSH6*, *MLH1*, and *PMS2*). The diagnosis of LS is often challenged by the identification of missense mutations, termed variants of uncertain significance, whose functional effect on the protein is not known. Of the eight PMS2 variants initially selected for this study, we identified a variant within the N-terminal domain where asparagine 335 is mutated to serine, p.Asn335Ser, which lacked ATPase activity, yet appears to be proficient in MMR. To expand our understanding of this functional dichotomy, we performed biophysical and structural studies, and noted that p.Asn335Ser binds to ATP but is unable to hydrolyze it to ADP. To examine the impact of p.Asn335Ser on MMR, we developed a novel in-cell fluorescent-based microsatellite instability reporter that revealed p.Asn335Ser maintained genomic stability. We conclude that in the absence of gross structural changes, PMS2 ATP hydrolysis is not necessary for proficient MMR and that the ATPase deficient p.Asn335Ser variant is likely benign.

KEYWORDS
ATPase activity, fluorescent-MSI reporter, isothermal titration calorimetry, Lynch syndrome, PMS2 p.Asn335Ser, variants of uncertain significance, X-ray crystallography

1 | INTRODUCTION

The mismatch repair (MMR) pathway is a highly conserved, post-replicative DNA repair pathway necessary for correcting single base mismatches and insertion–deletion (indel) loops, which increases the overall fidelity of replication by ~50–1000-fold (reviewed in [Buermeyer et al., 1999; Hsieh & Yamane, 2008; Kunkel & Erie, 2015; Li, 2008; Modrich & Lahue, 1996]). In humans, initiation of MMR occurs following the identification of a DNA mismatch by MutSα (a heterodimeric complex of MSH2 and MSH6; identifies base–base mismatches and small indels) or MutSβ (a heterodimeric complex of MSH2 and MSH3; identifies larger indels). MutSα recruits a second heterodimer, MutLα (complex of MLH1 and PMS2). PMS2 has latent endonuclease activity that is stimulated by the interaction with proliferating cell nuclear antigen (PCNA), replication factor C (RFC), MutSα, and ATP (Genschel et al., 2017; Kadyrov et al., 2006). The resulting DNA nick allows exonuclease 1 (Exo1) to resect the DNA surrounding the mismatch, creating an extended patch of ssDNA that is stabilized through interactions with replication protein A (RPA) (Myler et al., 2016). This is followed by the recruitment of Polδ and DNA ligase to replicate and join the DNA strands, respectively, to complete the repair process (Longley et al., 1997; Schofield & Hsieh, 2003).

Heterodimeric MutLα in humans differs from its prokaryotic MutL homolog in that the latter functions as a homodimer (Li & Modrich, 1995; Prolla et al., 1998). Structural and functional studies reveal that the N-terminal domain of MutL and its homologs contain an ATPase domain, belonging to the GHKL ATPase superfamily (Dutta & Inouye, 2000). This family of proteins is named after the members that make up this protein class (DNA gyrase B, Hsp90, bacterial histidine kinase, mitochondrial serine kinase, and MutL). The crystal structure of the unliganded N-terminal domain of bacterial MutL revealed that a portion (approximately one-fifth) of the protein is disordered; however, several of the disordered loops are highly conserved through species (Ban & Yang, 1998). The binding of ATP and its subsequent hydrolysis causes large conformational changes in MutL where the regions of disorder become ordered and this structural rearrangement further allows for downstream proteins to interact with MutL throughout the MMR process (Ban et al., 1999; Junop et al., 2003). The crystal structures of the N-terminal ATPase domains of PMS2 and MLH1 were also solved in the presence and absence of adenine nucleotides and its non-hydrolyzable analogs (Guarne et al., 2001; Wu et al., 2015). Mutation of highly conserved residues within the ATPase active site of MLH1 resulted in an increase in aberrant MMR and microsatellite instability (MSI), whereas equivalent active site mutations in PMS2

appeared to have no effect on MMR function indicating a variable contribution of the two ATPase domains to MMR (Johnson et al., 2010). Furthermore, while PMS2 requires MLH1 binding to form a stable heterodimeric MutLα complex, MLH1 can bind to alternate partners including PMS1, MLH3, and MBD4 (Bellacosa et al., 1999; Kondo et al., 2001). As such, the loss of PMS2 results only in the lack of PMS2 and does not appear to result in the complete loss of MLH1 expression. Conversely, a functional defect in MLH1 results in PMS2 instability and leads to a loss of expression of both proteins (Hinrichsen et al., 2017; Lynch et al., 2015; Mohd et al., 2006; Perera & Bapat, 2008).

The importance of the MMR pathway is underscored by the fact that inherited loss-of-function mutations in _PMS2_ (OMIM accession number: *600259), _MLH1_ (OMIM accession number: *120436), _MSH2_ (OMIM accession number: *609309), or _MSH6_ (OMIM accession number: *600678) often cause MSI and a hypermutable phenotype resulting in an autosomal dominant hereditary cancer condition known as Lynch syndrome (LS) (Buermeyer et al., 1999; Fishel & Kolodner, 1995; Kolodner, 1996; Lynch et al., 2015; Modrich & Lahue, 1996; Peltomaki, 2001; Peltomaki & Vasen, 1997). Patients with LS have a predisposition to cancers of the colon, endometrium, gastric, and other tissues. Variants identified through germline analysis are classified as pathogenic, likely pathogenic, variant of uncertain significance (VUS), likely benign, or benign, per the ACMG recommended guidelines for sequence interpretation (Richards et al., 2015). VUSs account for 20%–30% of the noncoding and missense mutations in individuals undergoing genetic testing for LS and place ambiguity on proper clinical diagnosis and medical management.

Previously, we used in vitro and structural approaches to study two VUSs located within the N-terminal domain of PMS2 (D'Arcy et al., 2019). Within the clinical context of genetic counseling and testing at the Mitchell Cancer Institute (Mobile, AL), we previously identified a _PMS2_ variant that resulted in a protein where three amino acids were deleted in the ATP-binding site of PMS2, p.Leu42_Glu44del. The resulting protein lacked ATPase activity, structural integrity, and MMR activity. In the current study, to validate the robustness of our assays and to confirm good agreement with previously established findings, we selected several VUSs located in both the N- and C-terminal domains of _PMS2_. After observing that one variant, p.Asn335Ser, exhibited in vitro evidence of MMR efficiency while lacking ATPase activity, we focused the remainder of our efforts on characterizing this particular variant using biophysical and structural approaches. Collectively, our data suggest that PMS2 ATPase activity is not necessary for the role of MutLα during MMR but is contingent upon the ATPase domain remaining structurally intact.

2 | METHODS

2.1 | Plasmids, protein expression, and purification

The pET15b-PMS2 expression construct encodes the N-terminal residues (1–365) of PMS2 and was kindly provided by Dr. Wei Yang (National Institute of Health). pSG5 PMS2-WT (pSG5 PMS2-wt was a gift from Bert Vogelstein (Addgene plasmid # 16475; http://n2t.net/addgene:16475;RRID:Addgene_16475) [Nicolaides et al., 1998]) harboring full-length PMS2 (GenBank Reference Sequence #NG_008466.1) and pCEP9 MLH1 (pCEP9 MLH1 was a gift from Bert Vogelstein (Addgene plasmid # 16458; http://n2t.net/addgene:16458;RRID:Addgene_16458) [Papadopoulos et al., 1994]) harboring full-length MLH1 (GenBank Reference Sequence #NG_007109.2) were obtained from Addgene. The PMS2 p.Val816Glu, p.Glu705Lys, p.Asp699His, p.Gly779Arg, p.Arg799Gln, p.Gly232Glu, p.Ser238Arg, or p.Asn335Ser variants were generated with the Quikchange II XL site-directed mutagenesis kit (Agilent Technologies) following the manufacturer's protocol and propagated in XL10 Gold *E. coli*. Primer sets to generate the variants were as follows: p.Val816Glu forward primer 5′-ctgccggaagtcggag atgattgggactg-3′ and reverse primer 5′-cagtcccaatcatctccg acttccggcag-3′; p.Glu705Lys forward primer 5′-accagcatg ccacggacaagaagtataacttcgag-3′ and reverse primer 5′-ctc gaagttatacttcttgtccgtggcatgctggt-3′; p.Asp699His forward primer 5′-aggatatcttcatagtgcaccagcatgccacgga-3′ and reverse primer 5′-tccgtggcatgctggtgcactatgaagatatcct-3′; p.Gly779Arg forward primer 5′-aaaaactggaccttcagaccccca ggacgtcg-3′ and reverse primer 5′-cgacgtcctggggtctgaaggt ccagtttt-3′; p.Arg799Gln 5′-ggggtcatgtgccagccttcccgagtc-3′ and reverse primer 5′-gactcgggaaggctggcacatgacccc-3′; p.Gly232Glu forward primer 5′-tatcggctctgtgtttgagcagaag cagttgcaaa-3′ and reverse primer 5′-tttgcaactgcttctgctcaaa cacagagccgata-3′; p.Ser238Arg forward primer 5′-gcagaag cagttgcaaaggctcattccttttgttcag-3′ and reverse primer 5′-ct gaacaaaaggaatgagcctttgcaactgcttctgc-3′; and p.Asn335Ser forward primer 5′-atttctgttgattcagaatgcgttgatatcagtgttact ccagataaa-3′ and reverse primer 5′-tttatctggagtaacactgata tcaacgcattctgaatcaacagaaat-3′. The nucleotide sequences of wild-type (WT) and variant constructs were verified by DNA sequencing (Eurofins).

As described previously (D'Arcy et al., 2019), the 6× histidine (His)-tagged WT and variant forms of the N-terminal domain of PMS2 were expressed in *E. coli* Rosetta 2 (DE3) cells (Novagen) following induction by isopropyl-β-D-thiogalactopyranoside (IPTG) at 18°C for 18 h. Cells were lysed in the presence of 1 mM phenylmethylsulfonyl fluoride (PMSF) and 1× cOmplete EDTA-free protease inhibitor cocktail (Roche). Protein was purified on two HiTrap TALON crude columns (GE Healthcare, 1.6 × 2.5 cm) in 10 mM potassium phosphate pH 6.3, 150 mM potassium chloride, 5% glycerol, 20 mM imidazole, and 2 mM β-mercaptoethanol with an imidazole gradient followed by a HiTrap QFF column (GE Healthcare, 1.6 × 2.5 cm). Thrombin was used to cleave the His-tag from the protein and the protein was then passed through a HiTrap SPFF column (GE Healthcare, 1.6 × 2.5 cm). Protein preps were concentrated to ~7.5 mg/ml and flash cooled in liquid nitrogen for long-term storage.

2.2 | ATPase activity assay

A malachite green/molybdate-based colorimetric assay (Biomol Green reagent, Enzo Life Sciences) was used to assess ATPase activity as described previously by us and others (D'Arcy et al., 2019; Rule et al., 2016). Briefly, reactions containing 20 µM enzyme were assembled in 20 mM HEPES pH 8.5, 13 mM NaCl, 1% glycerol, 5 mM ATP, and 5 mM $MgCl_2$ in a total volume of 30 µl. Reactions were initiated by the addition of ATP and $MgCl_2$, and at the indicated time points (0, 15, 30, 45, and 60 min), 5 µl aliquots were removed and quenched by diluting into 245 µl 1 × HNG buffer followed by flash freezing in liquid nitrogen. To determine the amount of orthophosphate released, Biomol green reagent was added to each well and absorbance was measured at 620 nm using a Tecan Infinite M1000 Pro multimode plate reader. The mean ± *SEM* was derived from the cumulative data generated from three separate experiments.

2.3 | Cell culture and transfection

HCT116 cells were acquired from ATCC (CCL-247) and cultured in HyClone McCoy's 5a medium modified (GE Healthcare Life Sciences) supplemented with 10% fetal bovine serum (Atlanta Biologicals), 50 U penicillin, and 50 µg/ml streptomycin (Gibco). Cultures were maintained at 37°C in a 5% CO_2 humidified atmosphere. Cells were co-transfected using pSG5 PMS2-WT (Addgene Plasmid #16475), p.Val816Glu, p.Glu705Lys, p.Asp699His, p.Gly779Arg, p.Arg799Gln, p.Gly232Glu, p.Ser238Arg, or p.Asn335Ser variant concomitantly with pCEP9 MLH1 (Addgene plasmid #16458). As we previously reported (D'Arcy et al., 2019), the pSG5 PMS2-WT plasmid acquired from Addgene contained a missense mutation at lysine 541, p.Lys541Glu. The p.Lys541Glu mutation was reverted to the consensus WT sequence using the Quikchange II XL site-directed mutagenesis kit with forward primer 5′-aaaagagtcgtcagttttaggcgctttctcctgag-3′ and reverse primer 5′-ctcaggagaaagcgcctaaaactgacgactctttt-3

'. Using the modified pSG5 PMS2-pGlu541Lys plasmid, p.Val816Glu, p.Glu705Lys, p.Asp699His, p.Gly779Arg, p.Arg799Gln, p.Gly232Glu, p.Ser238Arg, and p.Asn335Ser variant plasmids were generated using the primer sets described above. HCT116 cells were seeded (eight 150 mm culture dishes per construct for MMR assays with nuclear extracts, one 150 mm culture dish per construct for western blots of nuclear extracts, or one 100 mm culture dish for whole cell extracts) and grown to 70% confluency prior to transient transfection with the PMS2 and MLH1 expression plasmids. Cells were transfected with 2.5 µg (100 mm dish) or 7 µg (150 mm dish) of each plasmid with a 1:6 ratio of PEI (1 mg/ml; Polysciences, MW 25,000, Linear) and cultured for an additional 48 h prior to harvesting.

2.4 | SDS-PAGE and Western blot

SDS-PAGE and western blots were performed as described previously (D'Arcy et al., 2019). Antibodies used for the western blots include: PMS2 mouse monoclonal antibody (1:1000; Santa Cruz Biotechnology, Cat # sc-25,315) and MLH1 mouse monoclonal antibody (1:1000; Santa Cruz Biotechnology, Cat # sc-133,228 X). For the loading control, PCNA, a (D3H8P) XP rabbit monoclonal antibody (1:1000; Cell Signaling, Cat #13110S) was used. An ECL anti-mouse IgG secondary antibody conjugated to horseradish peroxidase (HRP) (1:10,000, GE Healthcare NA931VS, from sheep) or anti-rabbit IgG secondary antibody conjugated to HRP (1:10,000, GE Healthcare NA934V, from donkey) and Advansta Inc Westernbright Sirius—femtogram substrate were used to visualize antibody binding using a Bio-Rad ChemiDoc imager. As performed previously, relative PMS2 expression was quantified and normalized to PCNA using ImageLab 5.2.1 software (Bio-Rad). The mean ± *SEM* was derived from the cumulative data generated from three separate experiments. Statistical analysis was performed in GraphPad Prism 7 using an unpaired t-test with Welch's correction where equal standard deviations are not assumed.

2.5 | Nuclear extract preparation and in vitro mismatch repair assays

Nuclear extracts were prepared with minor modifications to the original methods (Geng et al., 2011) and as we have previously described in detail (D'Arcy et al., 2019). The MMR assays performed were also previously described in (D'Arcy et al., 2019). Briefly, reactions containing 100 µg of nuclear extract, 100 ng of pUC19HXB DNA substrate, 0.1 mM of dNTPs in the standard MMR buffer were assembled in a total volume of 40 µl and incubated

at 37°C for 1 h. The reaction was terminated by the addition of 80 µl of stop solution containing proteinase K and incubated for an additional 30 min at 37°C. DNA was isolated by extraction sequentially with phenol, phenol/chloroform/iso-amyl alcohol, and chloroform. The DNA was digested with AseI and XhoI restriction enzymes (NEB), and was separated by electrophoresis on a 1% agarose gel. Agarose gels were stained with SYBR GOLD for 20 min and destained in 1X TAE prior to being imaged with a Bio-Rad ChemiDoc imager. ImageLab 5.2.1 software (Bio-Rad) was used to assess repair yield. The repair yield is equivalent to the ratio of the summed intensities of the 759 bp and 1216 bp fragments to the total intensities of the 759 bp, 1216 bp, and 1975 bp bands. Repair assays were conducted in triplicate and graphed as the mean ± *SEM*. Statistical analysis was performed in GraphPad Prism 7 using an unpaired t-test with Welch's correction where equal standard deviations are not assumed.

2.6 | Differential scanning fluorimetry

Differential scanning fluorimetry (DSF) was performed using the Prometheus NT.48 instrument (NanoTemper Technologies, LLC, South San Francisco, CA) with 48 capillary chambers. Each sample was excited at 290 nm and intrinsic fluorescence emission was detected simultaneously at 330 (F_{330nm}) and 350 nm (F_{350nm}). Thermal unfolding was performed in Buffer B (20 mM HEPES pH 7, 150 mM KCl, 5% glycerol, and 1 mM TCEP) with a total volume of 10 µl per sample capillary. Melting curves were recorded from 15 to 95°C with a constant heating rate of 2°C/min. Triplicate measurements were performed on each sample. Tm of each sample was automatically determined by the built-in analysis software and tabulated in an Excel output file.

2.7 | Isothermal titration calorimetry

Binding constants, stoichiometry, and heat of binding between PMS2 WT and p.Asn335Ser variant for ATP were evaluated using the MicroCal Auto-ITC200 System (Malvern Instruments, Westborough, MA) at the University of Alabama at Birmingham (UAB) Comprehensive Cancer Center's core facility. Protein preparations of the N-terminal ATPase domain of PMS2 WT (171, 165, and 226 µM) and p.Asn335Ser variant (180, 119, and 163 µM) were prepared as described above. Protein was buffer exchanged into Buffer B (20 mM HEPES pH 7, 150 mM KCl, 5% glycerol, and 1 mM TCEP) by size exclusion chromatography and

concentrated to the indicated concentration using an Amicon Ultra-15 10 kDa cutoff centrifugal filter. ATP (10 mM) was suspended in Buffer B and adjusted to pH 7 with NaOH. Prior to snap freezing in liquid nitrogen, samples were filtered with Corning Costar Spin-X centrifuge tube filters (0.22 μm pore size, cellulose acetate membrane, Millipore Sigma). Samples were thawed on ice and 6 mM $MgCl_2$ was added to the protein, ligand, and buffer prior to the titration experiments. The titrations were carried out at 10°C with 16 injections of 2.5 μl ATP (30-fold molar excess). An additional first injection of 0.2 μl was included to eliminate potential dilution of the titrant at the tip of the syringe. Background mixing heat was determined from injections of ATP into the same buffer without protein. Data analysis was performed using the ITC analysis module in Origin 7 (OriginLab, Northampton, MA). The normalized titration heat after subtraction of background mixing heat was fitted to a "one set of sites" model to determine the best-fit binding parameters. ITC measurements were performed in triplicate.

2.8 | Protein crystallization and structure determination

2.8.1 | Crystallization and data collection

Crystals of the PMS2 WT and p.Asn335Ser variant were obtained using hanging drop vapor diffusion methods at 16°C in conditions containing 8% tacsimate pH 5.8 (v/v) and 25% PEG 3350 (w/v). The concentrated protein (7.5 mg/ml) was combined with the crystallization reagent in a 1:1 ratio. Crystals were obtained after ~7 days and ATP soaks were performed by incubating crystals with 10 mM ATP/$MgCl_2$ for 1 h. Crystals were mounted onto MiTeGen micro loops and flash cooled by plunging into liquid nitrogen. The PMS2 p.Asn335Ser Apo structure was collected in-house using an IμS 3.0 microfocus source (INCOATEC) and PHOTON II CPAD detector (Bruker). Data (120 s per exposure) were collected to 2.0 Å with a crystal-to-detector distance of 50 mm and an image width of 0.2° per frame. The PMS2 WT and p.Asn335Ser ATP structures were collected at the Advanced Photon Source (APS Beamline 23-ID-B; Argonne, IL) with a Dectris Eiger 16 M detector at 12kEv. Data (0.25 s per exposure) for the WT and p.Asn335Ser ATP structures were collected to 2.04 Å and 2.12 Å, respectively, with a crystal-to-detector distance of 300 mm and an image width of 0.2° per frame. The data were processed and reduced using the PROTEUM III program suite (Bruker, AXS). Data collection statistics are summarized in Table S3.

2.8.2 | Structure determination and refinement

Orthorhombic pseudo-merohedral twinned crystals of p.Asn335Ser belong to the $P2_12_12_1$ space group and contained two molecules per asymmetric unit. The crystals calculated solvent content ranged from 47% to 47.5%. The structures of the PMS2 WT and p.Asn335Ser were solved by molecular replacement with Phaser-MR (Adams et al., 2010) using the crystal structure of the N-terminal domain of PMS2 (PDB: 1H7S) as a starting model (Guarne et al., 2001). Refinement was performed with Phenix. Refine (Afonine et al., 2012) using the twin law operator k,h,-l. Model building and map fitting were performed in COOT (Emsley et al., 2010). Water molecules were updated during refinement and manually checked. The final model for the structure was found to exhibit good geometry, as determined using MolProbity (PHENIX; [Chen et al., 2010]). Refinement statistics are shown in Table S3. All structure figures were prepared using PyMOL (The PyMOL Molecular Graphics System, Version 1.7.6 Schrödinger, LLC).

2.9 | Protein data Bank accession code

Atomic coordinates and structure factor amplitudes have been deposited with the protein data bank (http://www.pdb.org) and are accessible under accession code 7RCB (PMS2 p.Asn335Ser Apo), 7RCI (PMS2 p.Asn335Ser ATP), 7RCK (PMS2 WT ATP).

2.10 | HEK-293 PMS2 Knock out cell line generation

HEK-293 (Clontech) cell lines were cultured in Dulbecco's Modified Eagle Medium (DMEM), containing 25 mM D-glucose, 4 mM L-glutamine, 1 mM sodium pyruvate, 100 units/ml penicillin, 100 μg/ml streptomycin (Gibco, Life Technologies), and 10% fetal bovine serum (Atlanta Biologicals, Lot# C19032) at 37°C with 5% CO_2 in a humidified incubator. To generate HEK-293 PMS2 KO cells, the IDT Alt-R CRISPR-Cas9 system protocol using the Neon transfection system (Invitrogen) was employed with the following modifications. Briefly, The CRISPOR (v4.92) web tool (Concordet & Haeussler, 2018) was used to identify *Sp*Cas9 guide RNAs (gRNAs) to introduce DSBs into exon 1 and 2 of *PMS2*. Five gRNAs were selected based on predicted on- and off-target scoring, synthesized as synthetic gRNAs containing phosphorothioate modifications (crRNA:tracrRNA duplex; Invitrogen A35512

and A35507, respectively) and generated as two independent oligonucleotides that were annealed according to the manufacturer's standard protocol. For each electroporation, the Alt-R Cas9 enzyme (10 mg/ml) was diluted to 5.8 mg/ml with resuspension buffer R from the Neon system kit. The RNP complex was formed by incubating the Cas9 enzyme (0.5 µl) with the gRNA (0.5 µl; 22 pmol) at RT for 15 min.

HEK-293 cells were pelleted and washed with 5 ml of 1× PBS. The PBS was decanted, and cells were suspended in 1 ml PBS. Cell number was assessed using a Countess II FL cell counter (Life Technologies) and 2×10^5 cells were aliquoted into a 1.5 ml microcentrifuge tube and pelleted. Cells were suspended in 9 µl of resuspension buffer R and the RNP complex (1 µl) and 10.8 µM Alt-R Cas9 electroporation enhancer (2 µl) were added to the cell suspension. The RNP was electroporated into HEK-293 cells using the Neon transfection system following the manufacturer's protocol with 2 pulses, 20 ms at 1300 V and seeded into 6-well plates prefilled with 5 ml DMEM supplemented with 10% FBS and given 72 h to recover.

To determine the gRNA with the highest on-target efficiency, genomic DNA from cells electroporated with each gRNA was isolated using the GeneJet genomic DNA purification kit (Thermo Scientific). Genomic DNA (500 ng) was used to amplify PMS2 exon 1 and exon 2 using primers specific for the coding *PMS2* locus (Nicolaides et al., 1995). Polymerase chain reaction of PMS2 exon 1 was performed using the Q5 hot start high-fidelity polymerase master mix (NEB) with 10 µM forward (5′-ggtcacgacggagaccg-3′) and 10 µM reverse primers (5′-ccatgttccccccatttcc-3′) using the manufacturer's standard protocol with the following modifications. Amplifications were performed at 98°C for 3 min for 1 cycle, then at 98°C for 10 s, 62°C for 30 s, and 72°C for 12 s for 35 cycles, and a final extension of 72°C for 2 min. Amplification products were Sanger sequenced using the exon 1 forward primer and the chromatograms were analyzed by sequence trace decomposition using TIDE analysis (Brinkman et al., 2014). Comparison of the on-target frequency within each cell population revealed a gRNA targeting exon 1 with 65% editing efficiency (gRNA targeting sequence: CGAGCUCUCAGCUCGCUCCA). The validated gRNA was used to generate HEK-293 PMS2 KO cells as described above. Following 72 h post electroporation, cells were single-cell sorted into clear 96-well plates (Costar) using a BD Biosciences FACS Aria II SORP high speed cell sorter from the entire population, expanded for single clone PCR-based screening using Sanger sequencing of exon 1 and Synthego ICE analysis (Synthego Performance Analysis, ICE Analysis. 2019. V2.0. Synthego; [March 10, 2020]).

2.11 | PMS2 WT, p.Asn335Ser, and p.Leu42_Glu44del lentiviral reintroduction

To generate stable HEK-293 cell lines expressing PMS2 WT, p.Asn335Ser, and p.Leu42_Glu44del, forward (5′-ggg gacaagtttgtacaaaaaagcaggctggcaccatggagcgagctgagagctcg-3′) and reverse (5′-ggggaccactttgtacaagaaagctgggttcagttctg agaaatgacacccag-3′) primers containing overhangs encoding attB recombination sites were synthesized and used to amplify full-length PMS2 WT and variants from the pSG5 constructs using Q5 hot start high-fidelity polymerase master mix (NEB) following the manufacturer's suggested protocol. The 2653 bp amplicons were agarose gel purified (Qiagen), cloned into pDonr221 using Gateway recombination, further subcloned into pLenti-CMV-Blast-Dest (706–1) (Campeau et al., 2009), and sequence verified.

Lentiviral particles encoding PMS2 WT, p.Asn335Ser, and p.Leu42_Glu44del constructs were produced with HEK-293FT cells using the third-generation lentiviral packaging system (Addgene # 12251, 12,253, and 12,259). Each transfer vector (3 µg pLenti-CMV-Blast (706–1)-PMS2 WT, p.Asn335Ser, and p.Leu42_Glu44del) and packaging vectors (7.5 µg pMDLg/pRRE, 3.75 µg RSV-REV, and 4.5 µg PMD2.G) were diluted with 1.875 ml Opti-MEM (1 µg plasmid DNA/100 µl Opti-MEM) in a glass vial. DNA was mixed gently prior to the addition of Xtreme Gene HP using a 1:3 (wt:vol) ratio of DNA to transfection reagent (56.25 µl). The mixture was gently mixed and incubated at room temperature for 20 min. Following incubation, the mixture was added to 10 ml of media, mixed by inversion, and added to a 0.10% gelatin coated T75 flask preseeded (2 $\times 10^6$ cells) with HEK-293FT cells grown to 70% confluency. Cells were allowed to produce lentiviral particles for 72 h. The viral supernatant was removed, debris pelleted (1625 × g) for 2 min, and filtered through a 0.45 µm polyethersulfone membrane using a syringe. The viral supernatant was aliquoted, flash frozen using liquid nitrogen, and stored at −80°C until needed.

HEK-293 PMS2 KO cells (2×10^6) were seeded into T75 flasks with 10 ml DMEM media supplemented with 10% FBS and cultured for 18 h. Cells were transduced with 0.5 ml of the viral supernatant incubated in 10 ml media with 10 µg/ml polybrene. Cells were cultured for 48 h prior to selection with 10 µg/ml blasticidin antibiotic for approximately two weeks. Stable PMS2 WT, p.Asn335Ser, and p.Leu42_Glu44del cell lines were single-cell cloned using a BD Biosciences FACS Aria II SORP high speed cell sorter from the entire population. Twelve clones from each group were expanded for genomic DNA isolation. The genomic DNA was isolated with the GeneJet genomic DNA purification kit (Thermo Scientific), and the lentiviral copy number for each clone was determined with the Lenti-X Provirus

Quantification Kit (Takara Bio USA) and a CFX96 Touch Real-Time PCR Detection System (Bio-Rad). Two clones from each group with an equivalent number of integrations (~20/cell) were further screened by western blotting to assess the relative PMS2 expression from nuclear extracts. Representative HEK-293 PMS2 WT, p.Asn335Ser, and p.Leu42_Glu44del clones demonstrating similar PMS2 expression levels were selected for further study.

2.12 | Construction and integration of a fluorescent microsatellite instability reporter

A fluorescent-based MSI reporter system was constructed by synthesizing DNA encoding mCherry and eGFP proteins separated by a mononucleotide tract consisting of 27 guanines preceding an out-of-frame (OOF)-2A-ribosomal skipping peptide. When the microsatellite is intact (no MSI), the reporter constitutively expresses only the mCherry protein lacking its native stop codon with the C-termini fused to 9 glycines and 21 residues (QRRHQLQPAETGRGCGREPRP) from the OOF-2A peptide (including a GSG linker). To ensure eGFP expression is suppressed, the native start methionine was removed. The construct was synthesized (Genscript) with flanking attB Gateway recombination sites for cloning into pDonr221. The MSI reporter was further subcloned into pLenti-CMV-Puro-Dest (w118-1) and used to generate lentiviral particles as described above. Stable HEK-293 cell lines were derived using puromycin antibiotic selection (0.001 mg/ml) for two weeks prior to analysis.

2.13 | Microsatellite instability reporter analysis by flow cytometry

Prior to seeding, HEK-293 cell lines were enriched for mCherry positive eGFP negative fluorescence using a BD Biosciences FACS Aria II SORP high speed cell sorter using 488 nm laser excitation and 525/30BP detection for eGFP and 561 nm laser excitation and 610/20BP detection for mCherry. Following enrichment, cells were seeded (0.5×10^5) into 6-well plates containing 5 ml DMEM supplemented with 10% FBS and cultured for 96–120 h prior to passaging and analysis for mCherry/eGFP positive fluorescence. A subset of cells (0.5×10^5) from each passage were seeded into 6-well plates for subsequent passages. Leftover cells were analyzed on the FACS Aria II SORP as described above. The mean ± *SEM* was derived from the cumulative data generated from three technical replicates at each indicated cell passage. Statistical analysis was performed in GraphPad Prism 7 using a one-way ANOVA with Tukey's multiple comparisons post hoc test.

3 | RESULTS

3.1 | Selection of VUSs in current study

We evaluated eight VUSs identified within the *PMS2* gene (Table S1, Figures S1 and S2): c.2447 T > A, p.Val816Glu; c.2113G > A, p.Glu705Lys; c.2095G > C, p.Asp699His; c.2335G > A, p.Gly779Arg; c.2396G > A, p.Arg799Gln; c.695G > A, p.Gly232Glu; c.714C > A, p.Ser238Arg; c.1004A > G, p.Asn335Ser. Five of the variants (p.Val816Glu, p.Glu705Lys, p.Asp699His, p.Gly779Arg, p.Arg799Gln) are located in the C-terminal endonuclease domain that harbors a zinc-binding region where at least one of the two identified Zn^{2+} ions is coordinated within the endonuclease active site and interacts with MLH1 (Guarne, 2012; Hinrichsen et al., 2017; Kadyrov et al., 2006; Kosinski et al., 2008). The three remaining variants (p.Gly232Glu, p.Ser238Arg, p.Asn335Ser) are located in the N-terminal ATPase domain (Figure S2). To conduct in vitro expression, biochemical, and structural studies, we selected these variants based on (i) their location within either of the two structured N- and C-terminal domains of PMS2, (ii) past precedent in the literature to compare the validity and robustness of our assays; and lastly (iii) their current classification, where a majority of the selected variants are VUSs with limited biochemical characterization. Sequence conservation assessed by Align-GVGD indicate that seven of the eight selected variants are highly conserved whereas the p.Val816Glu variant displays intermediate conservation (Table S1, Figure S1). Population allele frequencies for each variant are displayed and range from 0.00001 to 0.00025 and are as high as 0.00046. Current ClinVar classification suggests that five of the eight variants are VUSs (p.Val816Glu, p.Gly779Arg, p.Arg799Gln, p.Gly232Glu, and p.Ser238Arg), one is pathogenic/likely pathogenic (p.Glu705Lys), and two variants have conflicting interpretations of pathogenicity (p.Asp699His and p.Asn335Ser). In this study, we use biochemical, biophysical, and structural experiments to evaluate the function of these variants.

### 3.2 | Expression of the PMS2 variants in human cells

Relative expression and stability of PMS2 WT, p.Val816Glu, p.Glu705Lys, p.Asp699His, p.Gly779Arg, p.Arg799Gln, p.Gly232Glu, p.Ser238Arg, and p.Asn335Ser was assessed using in vitro studies in HCT116 cells. HCT116

cells lack expression of MutLα due to hypermethylation of the MLH1 promoter resulting in the consequential loss of PMS2, whose stability is dependent on its interaction with MLH1 via the C-terminal domains of both proteins (Guarne, 2012; Hinrichsen et al., 2017). We transiently co-transfected identical amounts of plasmids encoding full-length PMS2 WT, p.Val816Glu, p.Glu705Lys, p.Asp699His, p.Gly779Arg, p.Arg799Gln, p.Gly232Glu, p.Ser238Arg, or p.Asn335Ser concomitantly with WT MLH1 and assessed relative protein expression after 48 h. Transfection of both PMS2 and MLH1 plasmids were required to observe overexpression of both proteins (Figure S3). Following transfection, the cells were harvested and the relative expression of PMS2 and MLH1 from nuclear (Figure 1a) and whole cell (Figure 1b) extracts were assessed by immunoblotting against both proteins. Quantification of the relative PMS2 WT and variant expression levels normalized to PCNA expression revealed a statistically significant reduction in the expression of p.Glu705Lys in both nuclear and whole cell extracts ($p < .01$). A reduction in expression was also previously observed when this conserved residue was mutated in mice, p.Glu702Lys (van Oers et al., 2010). Furthermore, in our experiments, we observed a concomitant reduction in MLH1 when coexpressed with p.Glu705Lys, suggesting the variant destabilizes the MutLα complex. Prior work with this variant indicates an inability to complement a mutator phenotype in PMS2$^{-/-}$ mouse embryo fibroblasts but does not show destabilization of the MutLα complex or reduced expression of the

variant itself (Deschênes et al., 2007). We also observed a statistically significant reduction in the expression of the p.Val816Glu variant in whole cell extracts ($p < .05$). Although not significant due to experimental variability, a similar reduction in p.Val816Glu from nuclear extracts was noted. The remaining three variants within the C-terminal domain and the three N-terminal variants do not appear to reduce the stability of the MutLα complex, and in some cases, PMS2 expression appears to be increased (e.g., p.Ser238Arg ($p < .05$) and p.Asn335Ser).
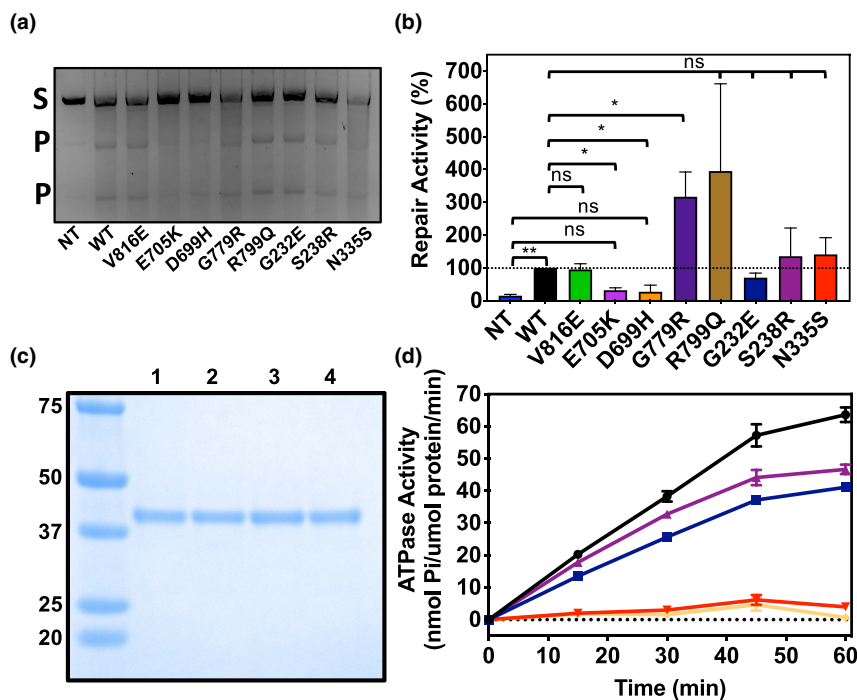
3.3 | MMR capacity of PMS2 WT and variant enzymes

The relative MMR activity of WT and variant PMS2 enzymes was assessed using the nuclear extracts from HCT116 cells and an in vitro DNA MMR assay that was described previously (D'Arcy et al., 2019). Nuclear extracts were incubated with a 1975 bp MMR substrate containing a single G-T mismatch at overlapping XhoI and HindIII restriction enzyme sites 144-bp away from a 3′ Nt.BstNBI nickase site. The 3′ nick, located on the sense strand containing the HindIII restriction enzyme site, directs the MMR machinery to correct the G-T mismatch to a canonical G-C base pair, restoring the XhoI restriction enzyme site. Double restriction enzyme digest with XhoI and AseI (a control restriction site) and electrophoresis of the digested products allow for quantification of the relative repair efficiency of the nuclear extracts
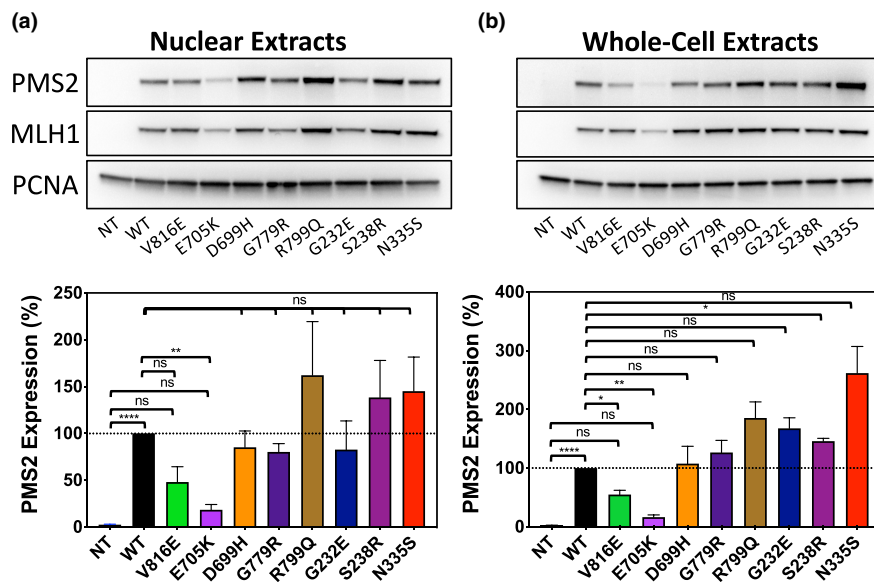
FIGURE 1 Transient expression of PMS2 p.Val816Glu and p.Glu705Lys is reduced compared to PMS2 WT. HCT116 cells were co-transfected with full-length MLH1 and PMS2 WT or variant plasmids. Following 48 h of incubation, nuclear and whole cell extracts were produced, and the relative expression levels were assessed by immunoblotting. Western blot analysis documenting the expression levels of PMS2 (non-transfected, WT, and variants), MLH1 WT, and PCNA from HCT116 (a) nuclear extracts and (b) whole cell extracts. Quantification of PMS2 WT and variant protein expression levels were normalized to the PCNA signal. The mean ± *SEM* was derived from the cumulative data generated from three separate experiments; ns, not significant, *$p < .05$, **$p < .01$, ***$p < .001$, ****$p < .0001$

FIGURE 2 Mismatch repair capacity of PMS2 p.Glu705Lys and p.Asp699His is reduced compared to PMS2 WT. (a) DNA agarose gel showing mismatch repair capacity of nuclear extracts from non-transfected, PMS2 WT, and variant transfected HCT116 cells incubated with pUC19HXB (100 ng) for 1 h. S and P refer to substrate and products, respectively. (b) Quantification of repair was assessed by measuring the relative signal of digested products to the total DNA. The mean ± *SEM* was derived from the cumulative data generated from three separate experiments; ns, not significant, *$p < .05$, **$p < .01$, ***$p < .001$, ****$p < .0001$. (c) Coomassie stained SDS-PAGE of purified His-tagged PMS2 WT (lane 1), p.Gly232Glu (lane 2), p.Ser238Arg (lane 3), and p.Asn335Ser (lane 4). d) ATPase activity of His-tagged PMS2 WT (black line), p.Gly232Glu (blue line), p.Ser238Arg (magenta line), and p.Asn335Ser (red line) protein preparations determined by a molybdate/malachite green-based ATPase activity assay. ATPase activity assessment of PMS2 WT and N-terminal variant proteins reveal the p.Asn335Ser variant is unable to hydrolyze ATP akin to the negative BSA control (pale orange line). The mean ± *SEM* was derived from the cumulative data generated from three separate experiments

from HCT116 cells expressing PMS2 WT or variant proteins (Figure 2a). Analysis of the repair yield (Figure 2b) revealed similar MMR activity between WT and the p.Val816Glu variant, despite the lower protein expression observed in the nuclear extracts (Figure 1a). In contrast, a statistically significant decrease in repair activity was observed with both the p.Glu705Lys and p.Asp699His variants. The pathogenic p.Glu705Lys variant was previously used as an MMR-deficient control using a cell-free assay to assess repair efficiency (Drost et al., 2013). The p.Asp699His variant, currently with conflicting classification of pathogenicity in ClinVar, was previously reported to have expression levels similar to WT with decreased protein function, as suggested similarly by our data (Huelsman et al., 2021). A majority of the reported evidence suggests that the p.Asp699His variant is likely pathogenic where Asp699 is present within the predicted zinc-binding motif in the endonuclease domain of PMS2 (Arora et al., 2017). Previous work by Modrich and others indicate that mutation of Asp699 to Asn results in a protein that lacks both endonuclease and MMR activities (Arora et al., 2017; Kadyrov et al., 2006; Kosinski et al., 2008). The p.Gly779Arg and p.Arg799Gln variants demonstrated

increased repair activity (~4 fold) compared to the WT control, revealing neither C-terminal variant had a negative impact on MMR activity. Likewise, the p.Gly232Glu, p.Ser238Arg, and p.Asn335Ser N-terminal variants demonstrated MMR efficiency comparable to control extracts.

3.4 | Expression, purification, and impact of N-terminal VUSs on ATPase function

Recombinant expression of full-length PMS2 is challenging, requiring co-expression with its binding partner MLH1 in insect or mammalian-based expression platforms. In addition to these expression systems being rather inefficient for producing large amounts of MutLα, structural analysis by X-ray crystallography has not been possible due to the high degree of disorder within the flexible linker of the full-length proteins. Despite these obstacles, it is relatively cost-efficient to produce milligram quantities of only the N-terminal domain of PMS2 using a bacterial expression system previously used to solve the crystal structure and test the ATPase activity of

PMS2 (Guarne et al., 2001). To our knowledge, no prior biochemical studies have been performed with the N-terminal p.Gly232Glu, p.Ser238Arg, and p.Asn335Ser variants and the latter variant has conflicting reports of pathogenicity, which warranted further investigation. We introduced the p.Gly232Glu, p.Ser238Arg, and p.Asn335Ser into a bacterial expression construct encoding the N-terminal domain of PMS2 (residues 1–365 [Guarne et al., 2001]) via site-directed mutagenesis and recombinantly expressed the variant proteins in *E. coli*. The WT and variant PMS2 proteins demonstrated good solubility and were easily purified to near homogeneity (Figure 2c). The N-terminal domain of PMS2 has been well characterized and is known to hydrolyze ATP to ADP and orthophosphate (P_i). Comparison of the ATPase activities of the recombinantly expressed PMS2 WT and variant proteins using a malachite green assay revealed the WT, p.Gly232Glu and p.Ser238Arg demonstrated a comparable time-dependent release of Pi from ATP (Figure 2d). In contrast, the ATPase activity of p.Asn335Ser was ablated, demonstrating similar ATPase activity to the negative control (BSA). These data suggest that introducing a serine at position 335 interferes with the ability of PMS2 to hydrolyze ATP to ADP + P_i.

3.5 | Differential scanning fluorimetry to assess protein stability of p.Asn335Ser

Nano differential scanning fluorimetry (nanoDSF; [Baljinnyam et al., 2020]) was used to determine the extent to which the p.Asn335Ser variant induced changes in the stability of the N-terminal domain of PMS2. Thermal unfolding was measured at F_{330nm} and F_{350nm} to determine whether differences in the thermal melting profiles were present. The melting profiles revealed at least two unfolding transitions were present; however, the second transition was not resolved from the first and deconvolution was not performed. There was no apparent difference in the stability between WT (Figure 3a; Tm1: 51.7 ± 0.2°C) and p.Asn335Ser (Figure 3b; Tm1: 51.6 ± 0.1°C) based on either F_{330nm} or F_{350nm}. To determine the extent to which ATP stabilized the N-terminal domain, we analyzed both proteins without ATP, with ATP alone, and ATP with MgCl2. From the results (summarized in Table S2), it was apparent that MgCl2 was required for ATP binding, as there was no change in the Tm by the presence of ATP alone (Tm1 for WT + ATP: 51.7 ± 0.0°C and N335S + ATP: 51.7 ± 0.2°C. The melting profiles revealed a lower Tm shift caused by 1 mM ATP/MgCl2 for the p.Asn335Ser variant (Tm1: 53.1 ± 0.1°C for the WT vs. 52.3 ± 0.1°C for the variant), which is consistent with the reduced affinity observed by isothermal titration calorimetry (ITC; discussed below). DSF results were corroborated by differential scanning calorimetry analysis, which also showed no apparent difference in stability and thermal unfolding profiles between WT and p.Asn335Ser (data not shown). In conclusion, DSF reveals that introducing a serine at position 335 in place of asparagine does not impact the overall stability of the N-terminal domain of recombinant PMS2.

3.6 | Assessment of ATP binding via calorimetric studies

To determine whether the loss of ATPase activity with the p.Asn335Ser variant was a consequence of an inability
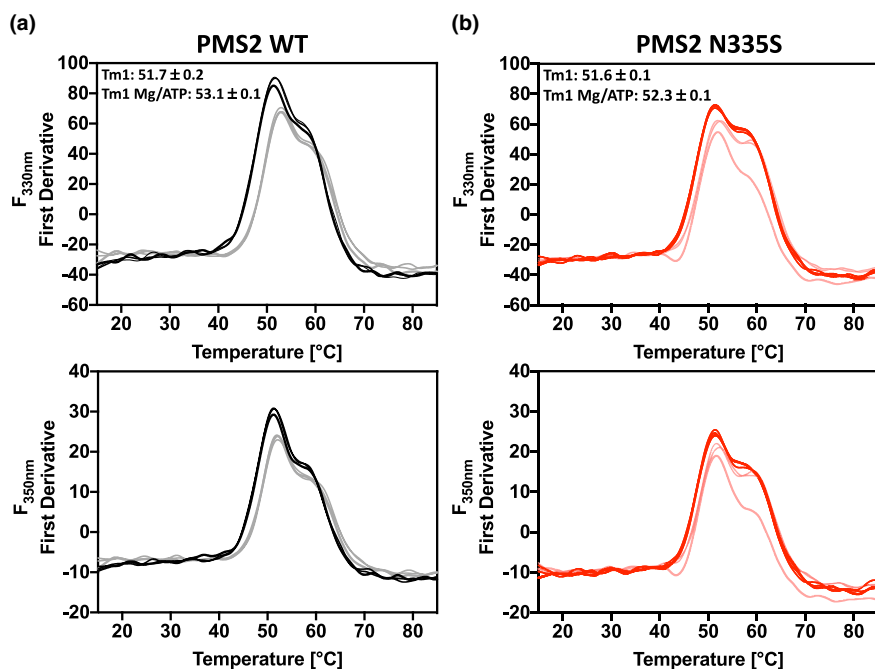

FIGURE 3 Differential scanning fluorimetry (DSF) reveals PMS2 stability is not impacted by the introduction of the p.Asn335Ser missense mutation. Thermal melting profiles of N-terminal (a) PMS2 WT and (b) PMS2 p.Asn335Ser were acquired at F_{330nm} and F_{350nm} with (gray/pink) and without (black/red) ATP/MgCl2 from 15 to 95°C with a constant heating rate of 2°C/min in triplicate. Tm1 values calculated based on F_{330} are listed within the figure and summarized in Table S2

to bind ATP, we evaluated the binding affinity of PMS2 WT and p.Asn335Ser with ATP using isothermal titration calorimetry (ITC). ATP was titrated resulting in a large, exothermic response for both WT (Figure 4a) and p.Asn335Ser (Figure 4b). The ITC thermograms were fitted with a one-site binding model resulting in molar binding stoichiometries of 1:1 for both proteins. We noted slower kinetics and a more negative enthalpy (ΔH) change for WT compared to p.Asn335Ser (-18.5 ± 0.9 vs. -13.8 ± 0.2 kcal/mol, respectively), which could in part be due to the additional heat released from ATP hydrolysis by WT. Moreover, the K_D was 1.75-fold lower for the WT compared to the p.Asn335Ser variant (mean of three experiments 0.059 mM and 0.103 mM, respectively). The higher ATP-binding affinity is in good agreement with our interpretation regarding the slower kinetics observed in the WT thermograms resulting from the hydrolysis of ATP. The decreased ΔH observed with the p.Asn335Ser variant was also associated with an unfavorable decrease in entropy change (ΔS, by -15.77 cal/[mol·K]) and a concomitant lowering in binding free energy change (ΔG) of -0.333 kcal/mol. The ITC experiments reveal the asparagine-to-serine mutation does not disrupt the binding of ATP, suggesting the loss of catalytic activity results from interference through an alternative mechanism.

3.7 | Structural evaluation of PMS2 WT and p.Asn335Ser by X-ray crystallography

We obtained diffraction-quality crystals for unliganded p.Asn335Ser and PMS2 WT and p.Asn335Ser complexed with ATP. The crystal structures were solved by molecular replacement using the N-terminal domain of PMS2 (PDB ID: 1H7S [Guarne et al., 2001]). The resolution of the three structures ranged between 2.0 and 2.12 Å, and the models were refined to a final R_{work} and R_{free} ranging from 0.1616 to 0.2226 and 0.1975 to 0.2475, respectively (Table S3). The crystal structures contain two molecules
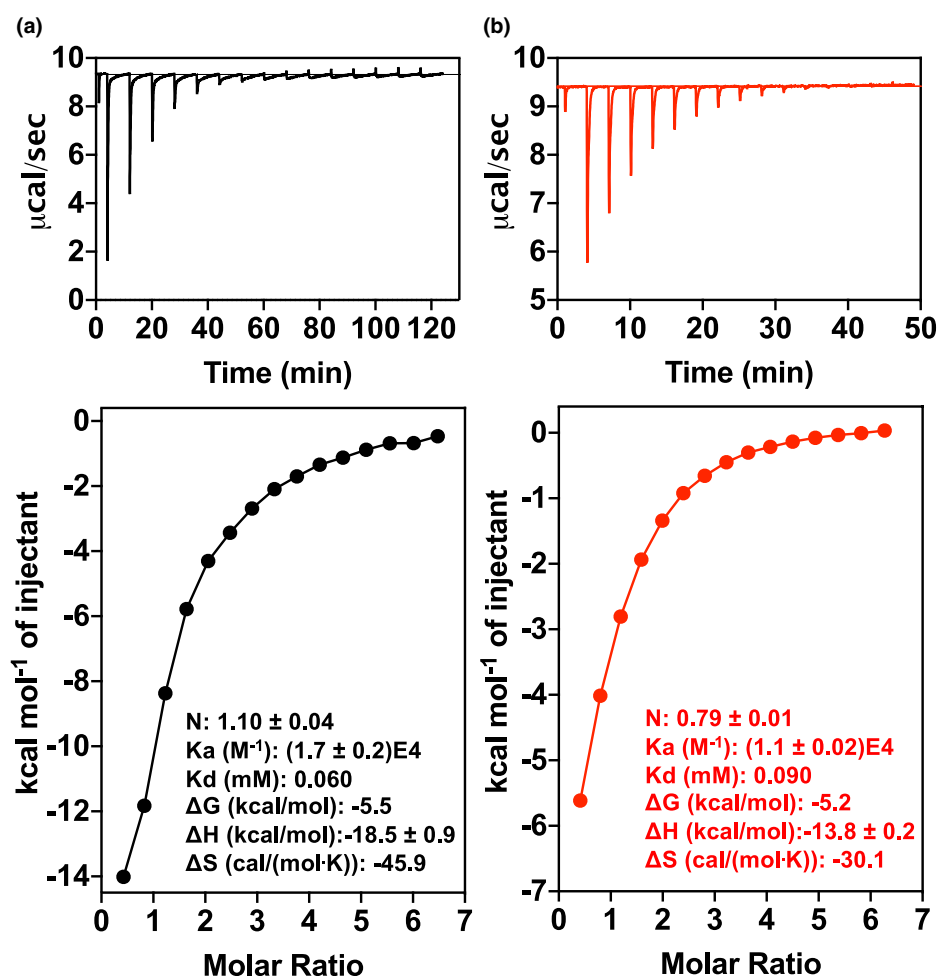

FIGURE 4 Isothermal titration calorimetry (ITC) reveals the p.Asn335Ser variant binds to ATP. (a) Raw ITC data and binding isotherms generated by plotting the integrated heat peaks against the molar ratio of the protein for (a) PMS2 WT (black) and (b) p.Asn335Ser (red) with ATP, respectively

per asymmetric unit, whereby each molecule is oriented antiparallel to the other with crystal packing contacts between the first α/β domain. Each molecule is composed of 365 residues and the average solvent content of the crystals was 47.2%. The PMS2 ATPase domain has an overall elbow-like shape resulting from the linkage of two α/β domains by two short alpha helices (residues 222–239) (Figure 5a). The first α/β domain comprising residues 1–221 consists of an eight-stranded mixed β-sheet packed against five α-helices. The second α/β domain (residues 239–365) is formed by a five-stranded mixed β-sheet with three α-helices forming a barrel that is capped by two β-strands. The second α/β domain is referred to as the transducer domain in some of the GHKL family members and contains a disordered loop comprising residues 334–343 (designated as loop L3 by [Guarne et al., 2001]), which extends towards the active site and positions a catalytically important lysine residue (Lys340) in close proximity to the γ-phosphate of ATP, stabilizing the transition state of ATP hydrolysis (Ban et al., 1999; Corbett & Berger, 2005). A lack of stabilizing intra- and intermolecular interactions results in disorder at the N-terminus of the construct (residues 1–33), the ATP lid (comprising residues 85–109), and residues

334–342, preventing several residues from being accurately modeled. Of the three current structures, Chain A of the N335S-ATP structure provides the greatest detail regarding the position of these disordered regions, lacking residues 1–29, residues 86–93, residues 106–108 of the ATP lid, and residues 336–342 in L3.

Liganded structures were obtained by soaking crystals with ATP/MgCl$_2$ for 1 h prior to mounting and flash cooling in liquid nitrogen. We observed clear electron density for ATP in the active site of both WT and p.Asn335Ser structures which were refined at full occupancy. We surmise that in the short duration of the soak, crystals of WT PMS2, which have a relatively slow rate of ATP hydrolysis were unable to hydrolyze ATP to ADP. Indeed, as previously, ATP hydrolysis *in crystallo* was observed between 4–12 h (Guarne et al., 2001). The structures of WT-ATP and N335S-ATP superimpose well onto the N335S-Apo structure (Figure 5a). The magnesium coordination sphere in the PMS2/ATP complex exhibits an octahedral geometry, interacting with Asn45, oxygen atoms from the α, β, and γ phosphates of ATP, and two water molecules. In the liganded structures, Glu42 adopts an alternative conformation coordinating with a γ-phosphate oxygen and one of two bridging water molecules (Figure 5b–d). The ATP/Mg^{2+}
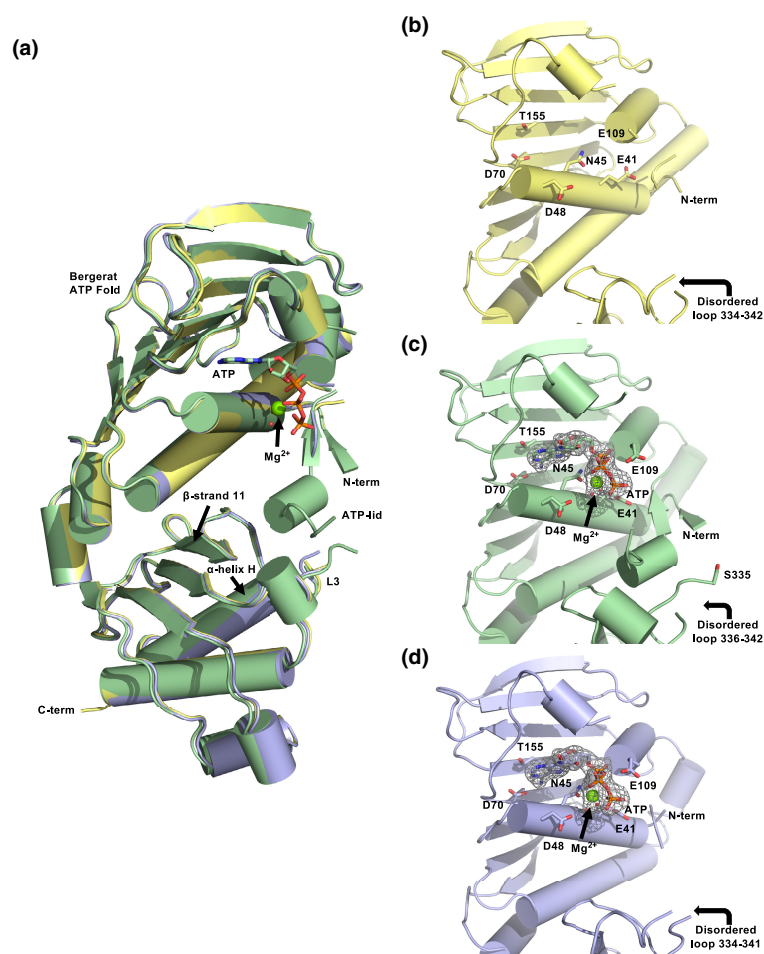
FIGURE 5 Crystal structures of the N-terminal ATPase domains of PMS2 p.Asn335Ser apo, p.Asn335Ser and WT complexed with ATP. (a) Superposition of PMS2 p.Asn335Ser apo (yellow; PDB ID: 7RCB), p.Asn335Ser-ATP (green; PDB ID: 7RCI), and WT-ATP (purple; PDB ID: 7RCK). The N-terminus, C-terminus, ATP, magnesium, and several other features are notated. Enlarged view of (b) p.Asn335Ser apo, (c) p.Asn335Ser-ATP, and (d) WT-ATP detailing key active site residues, ATP/MgCl$_2$, and the disordered loop containing amino acid 335. The composite omit map (autobuild; PHENIX) contoured at 1σ shows electron density for the ATP/MgCl$_2$ complex in gray

complex is further stabilized through interactions with the second bridging water molecule that is coordinated by Asn45 and Asp48.

Coordination of the adenine ring is mediated by hydrogen bonding interactions both directly and indirectly through a network of water molecules at the interface of the active site. Hydrogen bonding between Asp58 and the N6-amine acts as a major contributor for defining selectivity for ATP (Ban et al., 1999), while further stabilization is mediated through interaction of the adenine ring with Thr155 and Ser46.

In contrast to the unliganded p.Asn335Ser and WT-ATP structures, density for residues (94–105) of the ATP lid was apparent in the p.Asn335Ser-ATP structure. In the current crystal form, the ATP lid does not appear to directly interact with ATP but is positioned in a cleft formed between β-strand 14 of flexible loop 3 and a linker connecting β-strand 11 and α-helix H (Figure 5a). The p.Asn335Ser missense mutation is located in the disordered loop L3 which contains the important conserved Lys340 residue. Ser335 in the p.Asn335Ser-Apo structure (Figure 5b) and Asn335 in the WT-ATP structure (Figure 5d) exhibited high atomic displacement factors and were not modeled in the final structures. In contrast, there was sufficient density to model the S335 residue in the p.Asn335Ser-ATP bound structure (Figure 5c). The asparagine-to-serine mutation at position 335 replaces the carboxamide functionality of asparagine with a hydroxyl group from serine. Although we were able to model the position of the Ser335 residue, we were unable to identify residues that directly interacted with the serine hydroxyl due to the high degree of disorder in residues 336–342 (VTPDKRQ). Superposition of the p.Asn335Ser-ATP structure with the WT-ATP structure reveals the Ser335 missense mutation is positioned within hydrogen bonding distance to the backbone carbonyl and amide of Gln342 (3.2 Å and 3.3 Å, respectively).

3.8 | Generation of PMS2 knockout and stable cell lines

HEK-293 PMS2 knockout (KO or PMS2$^{-/-}$) cell lines were generated by disrupting exon 1 of *PMS2* using Cas9-induced double strand breaks (DSBs). PMS2 has 15 pseudogenes resulting from intrachromosomal duplications, 14 of which encode exons 1–5 (Blount & Prakash, 2018). As a result of the high number of pseudogenes, we screened five guide RNAs (gRNAs) to identify one with high efficiency for disrupting the functional endogenous coding *PMS2* gene. Using Cas9 from *S. pyogenes (SpCas9)* as a purified ribonucleic binding protein (RNP), we were able to identify a high efficiency gRNA targeting exon 1 of *PMS2*. The PMS2 KO gRNA introduces a DSB into codon 2 (amino

acid Glu2) of exon 1 (Figure S4a). Using *PMS2* coding-specific primers to amplify exon 1 (Nicolaides et al., 1995), Sanger sequencing, and analysis using sequence trace decomposition, we identified several homozygous and heterozygous PMS2 KO clones. Additionally, we were able to isolate several wild-type clones that were used as controls (Figure S4b). Clones were further validated by western blot analysis to confirm disruption of PMS2 expression (Figure 6a). These studies revealed that in the HEK-293 PMS2 homozygous KO (PMS2$^{-/-}$) and heterozygous (PMS2$^{+/-}$) cells, PMS2 expression was ablated or reduced by approximately 50% in each respective cell line when compared to PMS2 WT (PMS2$^{+/+}$) cells. Furthermore, we observed a 65% and 44% reduction in MLH1 expression in PMS2$^{-/-}$ and PMS2$^{+/-}$ cell lines, respectively.

To evaluate the effects of the p.Asn335Ser variant at the cellular level, homozygous PMS2 KO cells were used to generate stable overexpressing (OVR) cell lines using lentiviral transduction. The cell lines generated were p.Asn-335Ser^{OVR}, p.Leu42_Glu44del^{OVR} (known pathogenic N-terminal mutation from our previous studies [D'Arcy et al., 2019]), and WT^{OVR}. Stable cells were derived by blasticidin antibiotic selection, single-cell sorted to identify clones with equivalent viral copy numbers, and further screened for similar PMS2 expression levels (Figure 6b). Western blot analysis revealed that reintroduction of the full-length PMS2 constructs resulted in a 20-fold increase in expression when compared to endogenous levels of PMS2. In response to the increased levels of PMS2, we also observed a concomitant increase (maximum 14-fold) in MLH1 expression levels for both p.Asn335Ser^{OVR} and WT^{OVR} cells. However, expression levels for MLH1 were reduced in the p.Leu42_Glu44del^{OVR} cells, which aligns with our previous findings (D'Arcy et al., 2019). Due to the large increase in expression in the OVR cell lines compared to expression of endogenous MutLα, direct comparisons between the overexpression and endogenous cell lines were not made but were cross-referenced to each other relative to the PMS2$^{-/-}$ cell line.

3.9 | Microsatellite stability as a function of PMS2 status

To evaluate the impact of the PMS2 p.Asn335Ser VUS on MSI, we developed a novel in-cell fluorescent-based reporter system that detects microsatellite contractions through expression of enhanced green fluorescent protein (eGFP). The microsatellite instability (MSI) reporter encodes both mCherry and eGFP separated by a microsatellite consisting of 27 guanines and an out-of-frame 2A-ribosomal skipping peptide (Figure S5). Expression of eGFP is suppressed until the microsatellite contracts (−1

(a)

(b)

(c)
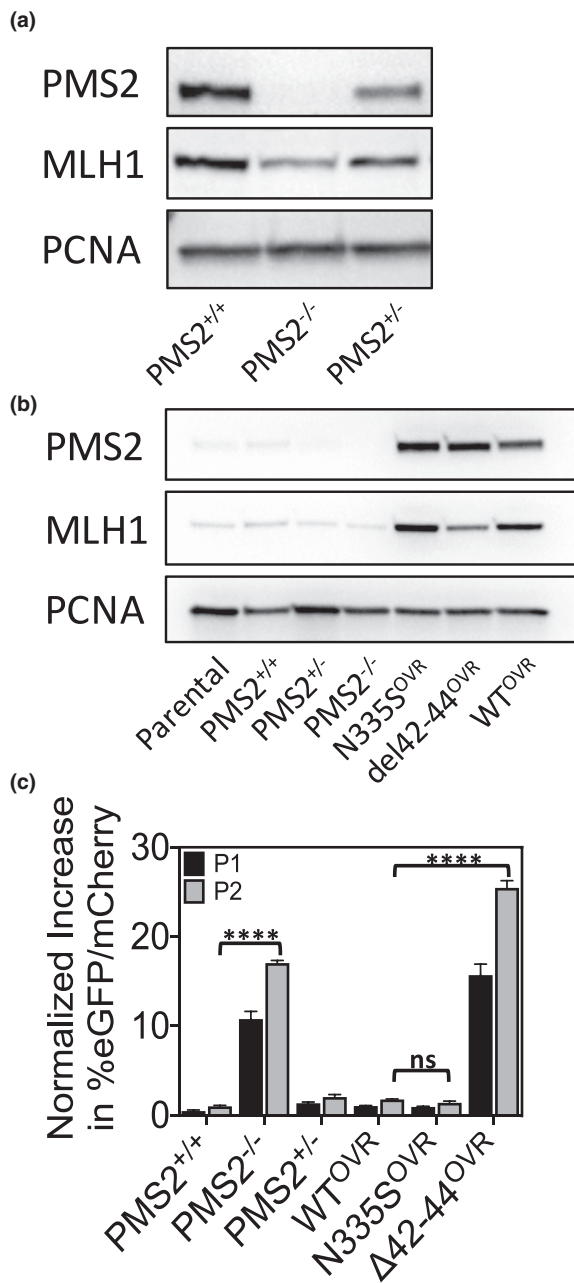
FIGURE 6 Cas9-induced disruption of PMS2 expression and assessment of PMS2 VUS impact on microsatellite stability via lentiviral reintroduction in HEK-293 cells. (a) HEK-293 PMS2 homozygous and heterozygous KO cell lines were generated through targeted disruption of _PMS2_ exon 1 by SpCas9. (b) Comparison of PMS2 and MLH1 expression levels in HEK-293 cell lines following integration and overexpression of PMS2-WT^{OVR}, p.Asn335Ser^{OVR}, and p.Leu42_Glu44del^{OVR} variants. (c) Longitudinal study documenting the accumulation of MSI in HEK-293 PMS2 cell lines expressing a fluorescent-based MSI-reporter. Statistical analysis was performed in GraphPad Prism 7 using a one-way ANOVA with Tukey's multiple comparisons post hoc test; ns, not significant, *$p < .05$, **$p < .01$, ***$p < .001$, ****$p < .0001$

frameshift), placing the 2A-ribosomal skipping peptide into frame, and resulting in the production of eGFP which was quantified using flow cytometry. As such, integration

of the MSI reporter into the altered HEK-293 PMS2 cell lines assisted in evaluating the pathogenicity of PMS2 VUSs as a function of MSI. In these studies, we evaluated the MSI status using stable cell lines OVR WT or variant PMS2 in cells lacking endogenous PMS2 (PMS2$^{-/-}$ background), which expressed the fluorescent MSI reporter. To determine the level of pathogenicity, we also overexpressed PMS2 WT, and PMS2 p.Leu42_Glu44del, which lacks ATPase activity and destabilizes the N-terminal domain of PMS2 (D'Arcy et al., 2019).

Longitudinal studies evaluating the percentage of PMS2$^{+/+}$ cells expressing eGFP revealed a 1.0% increase in eGFP following two successive passages (Figure 6c). In comparison, PMS2$^{-/-}$ and PMS2$^{+/-}$ cell lines acquired a 17.0% and 2.0% increase in eGFP, respectively. These data show that loss of PMS2 expression results in a large accumulation in MSI as compared to cells expressing endogenous WT PMS2. In contrast, the PMS2$^{+/-}$ cell line demonstrated a similar increase in eGFP to control PMS2$^{+/+}$ cells, suggesting reduction of PMS2 expression levels by 50% is sufficient to maintain microsatellite stability. Evaluation of the WT^{OVR} cell line revealed a 1.8% increase in eGFP after two successive passages, indicating reintroduction of PMS2 into the PMS2$^{-/-}$ cell line restores mismatch repair capacity. Similarly, the p.Asn335Ser^{OVR} cell line demonstrated a 1.4% increase in eGFP following the same number of passages, suggesting the VUS does not interfere with the cells' ability to maintain microsatellite stability and indicates the p.Asn335Ser is likely a benign variant. In contrast, p.Leu42_Glu44del^{OVR} cells demonstrated a 25.5% increase in eGPF, which was greater than the accumulation of eGFP observed in PMS2$^{-/-}$ cells. Although we were not able to determine the extent to which the results of the p.Leu42_Glu44del^{OVR} cells were influenced by the overexpression model, these data suggest that the presence of a pathogenic variant which results in destabilization of the N-terminal domain contributes to a more severe phenotype in comparison to missense mutations resulting in loss of PMS2 expression alone (i.e., premature stop codons).

4 | DISCUSSION

With our current work, we encountered the question regarding the degree to which MMR is dependent upon the ATPase activity of PMS2. We identified a variant in the N-terminal domain of PMS2 that resulted in the mutation of a highly conserved asparagine residue at codon 335 to serine where the recombinant N-terminal p.Asn335Ser displayed no ATPase activity, yet retained MMR activity in the context of the full-length enzyme. Our structural

studies comparing PMS2 WT and p.Asn335Ser complexed with ATP revealed two highly disordered regions corresponding to the ATP lid and loop L3. While these flexible regions were challenging to accurately model, previous studies from other members in the GHKL superfamily have shed light on their potential function (Corbett & Berger, 2003, 2005). Both PMS2 and MLH1 contain a Bergerat ATP-binding fold that facilitates the coordination of ATP (Dutta & Inouye, 2000). A unique feature of the Bergerat ATP-binding fold is that it lacks a catalytic basic residue necessary for breaking the phosphoanhydride bond of ATP's gamma phosphate to generate ADP. In other GHKL ATPases, the basic residue (lysine in type II topoisomerase and bacterial MutL [bMutL] or arginine in Hsp90) within the switch loop (loop L3 in PMS2) resides in a separate domain, designated the transducer domain, which is positioned in close proximity to the active site (Corbett & Berger, 2005). The conformational changes that the transducer domain and the essential switch loop undergo to place the switch lysine residue into and out of the active site is thought to cause an angular change in the positioning of the transducer domain, converting the chemical energy stored in ATP into mechanical motion (Corbett & Berger, 2003, 2005). In bMutL, the basic Lys307 residue, corresponding to Lys340 in PMS2, resides in a flexible loop and is highly conserved (Ban & Yang, 1998; Guarne et al., 2001). Ser335 is disordered in our crystal structures and is five residues away from this critical lysine residue. This essential lysine in bMutL (and other GHKL proteins) extends into the active site to stabilize the transition state of ATP hydrolysis (Ban et al., 1999). From these studies and our current data, we surmise that the introduction of Ser335 within the N-terminal domain of PMS2 reduces the conformational flexibility of the L3 loop, preventing Lys340 from participating as the catalytic basic residue required for the efficient hydrolysis of ATP.

Including p.Asn335Ser, ClinVar contains 13 missense germline variants within this disordered loop (residues 334–342). Twelve are still classified as VUSs while p.Asn335Ser has conflicting interpretations of pathogenicity; multiple laboratories classify p.Asn335Ser as a VUS and a minority of laboratories report it as benign or likely benign (Variant ID 127751). The interpretation of sequence variants identified in *PMS2* is challenging in part due to the lower penetrance of disease when compared to cancer risks reported in individuals with pathogenic *MLH1*, *MSH2*, and *MSH6* variants (Dominguez-Valentin et al., 2020; Senter et al., 2008; ten Broeke et al., 2018). Currently, monoallelic *PMS2* pathogenic mutations are believed to infer an approximate 2- to 4-fold increased risk of colorectal cancer and a 4- to 8-fold increased risk of endometrial cancer (National Comprehensive Cancer Network, 2021). Our experimental/functional studies

suggest that the p.Asn335Ser variant does not impact MMR activity and may not have a clinical impact. We utilized the guidelines for variant classification published by the American College of Medical Genetics and the Association for Molecular Pathology (Richards et al., 2015) to assess the criteria that the p.Asn335Ser variant meets for classification as either benign or pathogenic. There is evidence in the literature to suggest that p.Asn335Ser is benign where (i) segregation analysis for this variant in one family that met criteria for genetic testing for LS did not support pathogenicity (Hansen et al., 2017), and (ii) co-occurrence with a known pathogenic BRIP1 variant, which was reported elsewhere (Lerner-Ellis et al., 2021). There are also some evidence to suggest that this variant may be pathogenic including (i) an extremely low frequency of 0.0003% in population databases (ExAC frequency), which is well below the recommended 0.05% threshold for the frequency of a *PMS2* variant to be considered benign (Karczewski et al., 2020); (ii) identification of this variant in individuals or families with breast, ovarian, papillary thyroid, and colorectal cancer (Castéra et al., 2014; Maxwell et al., 2016; Mio et al., 2021; Rossi et al., 2017; Rummel et al., 2017; Stafford et al., 2017; Tung et al., 2015; Yurgelun et al., 2017); (iii) the asparagine residue is highly conserved across species; and (iv) multiple in silico software programs, which predict that this variant may impact protein function. However, this evidence does not meet the criteria for classification of a variant as a pathogenic. It is possible that p.Asn335Ser is benign with a low population frequency.

The impact of stable expression of p.Asn335Ser on MSI, a known clinical hallmark of LS, in cells lacking endogenous PMS2 expression was unremarkable. These data are in stark contrast to the p.Leu42_Glu44del variant we scrutinized previously, where three amino acids (Leu42, Val43, and Glu44) were deleted in the PMS2 N-terminal domain (D'Arcy et al., 2019). This previously studied deletion led to a loss of structural integrity in PMS2, resulting in a severely aggregated protein that lacked both ATPase and MMR functions. When we compared p.Asn335Ser to p.Leu42_Glu44del using our novel fluorescent MSI reporter, we noted a statistically significant increase in MSI only in the latter variant. From our current studies, we surmise that PMS2 ATPase activity is not necessary for its role during MMR as long as the ATPase domain remains structurally intact (i.e., the mutation does not disrupt any secondary structural elements within the PMS2 N-terminal domain). However, these studies do not delineate the role of PMS2 ATPase activity in cellular functions beyond MMR such as VDJ recombination, tumor suppression, class switch recombination, and interaction with additional factors such as p73 to enhance cisplatin-induced apoptosis (Péron et al., 2008; Shimodaira et al., 2003; van Oers et al., 2010). Given that PMS2 participates in pathways outside of canonical MMR, it

would be of value to identify and biochemically characterize a potential role for the residues within the flexible L3 loop via mutational analyses.

CONFLICT OF INTEREST

The authors state that there is no conflict of interest.

ETHICAL APPROVAL

This research does not involve human or animal subjects.

AUTHOR CONTRIBUTIONS

BD, JA, JW, V, SM, and ZY conducted the experiments; BD conceptualized the experiments, analyzed the data and prepared figures; BD, JB, and AP wrote the manuscript. All authors reviewed and approved the manuscript.

DATA AVAILABILITY STATEMENT

All structures have been deposited to the PDB and any other data that support the findings of this study are available from the corresponding author upon reasonable request.

ORCID

Aishwarya Prakash ![ORCID] https://orcid.org/0000-0003-1441-6237

REFERENCES

Adams, P. D., Afonine, P. V., Bunkóczi, G., Chen, V. B., Davis, I. W., Echols, N., Headd, J. J., Hung, L. W., Kapral, G. J., Grosse-Kunstleve, R. W., McCoy, A., Moriarty, N. W., Oeffner, R., Read, R. J., Richardson, D. C., Richardson, J. S., Terwilliger, T. C., & Zwart, P. H. (2010). PHENIX: A comprehensive python-based system for macromolecular structure solution. _Acta Crystallographica Section D, Biological Crystallography_, _66_(Pt 2), 213–221. https://doi.org/10.1107/S0907444909052925

Afonine, P. V., Grosse-Kunstleve, R. W., Echols, N., Headd, J. J., Moriarty, N. W., Mustyakimov, M., & Adams, P. D. (2012). Towards automated crystallographic structure refinement with phenix.Refine. _Acta Crystallographica Section D, Biological Crystallography_, _68_(Pt 4), 352–367. https://doi.org/10.1107/S0907444912001308

Arora, S., Huwe, P. J., Sikder, R., Shah, M., Browne, A. J., Lesh, R., Nicolas, E., Deshpande, S., Hall, M. J., Dunbrack, R. L., Jr., & Golemis, E. A. (2017). Functional analysis of rare variants in mismatch repair proteins augments results from computation-based predictive methods. _Cancer Biology & Therapy_, _18_(7), 519–533. https://doi.org/10.1080/15384047.2017.1326439

Baljinnyam, B., Ronzetti, M., Yasgar, A., & Simeonov, A. (2020). Applications of differential scanning fluorometry and related Technologies in Characterization of protein-ligand interactions. _Methods in Molecular Biology_, _2089_, 47–68. https://doi.org/10.1007/978-1-0716-0163-1_4

Ban, C., Junop, M., & Yang, W. (1999). Transformation of MutL by ATP binding and hydrolysis: A switch in DNA mismatch repair. _Cell_, _97_(1), 85–97. https://doi.org/10.1016/s0092-8674(00)80717-5

Ban, C., & Yang, W. (1998). Crystal structure and ATPase activity of MutL: Implications for DNA repair and mutagenesis. _Cell_, _95_(4), 541–552. https://doi.org/10.1016/s0092-8674(00)81621-9

Bellacosa, A., Cicchillitti, L., Schepis, F., Riccio, A., Yeung, A. T., Matsumoto, Y., Golemis, E. A., Genuardi, M., & Neri, G. (1999). MED1, a novel human methyl-CpG-binding endonuclease, interacts with DNA mismatch repair protein MLH1. _Proceedings of the National Academy of Sciences of the United States of America_, _96_(7), 3969–3974. https://doi.org/10.1073/pnas.96.7.3969

Blount, J., & Prakash, A. (2018). The changing landscape of Lynch syndrome due to PMS2 mutations. _Clinical Genetics_, _94_(1), 61–69. https://doi.org/10.1111/cge.13205

Brinkman, E. K., Chen, T., Amendola, M., & van Steensel, B. (2014). Easy quantitative assessment of genome editing by sequence trace decomposition. _Nucleic Acids Research_, _42_(22), e168. https://doi.org/10.1093/nar/gku936

Buermeyer, A. B., Deschenes, S. M., Baker, S. M., & Liskay, R. M. (1999). Mammalian DNA mismatch repair. _Annual Review of Genetics_, _33_, 533–564. https://doi.org/10.1146/annurev.genet.33.1.533

Campeau, E., Ruhl, V. E., Rodier, F., Smith, C. L., Rahmberg, B. L., Fuss, J. O., Campisi, J., Yaswen, P., Cooper, P. K., & Kaufman, P. D. (2009). A versatile viral system for expression and depletion of proteins in mammalian cells. _PLoS One_, _4_(8), e6529. https://doi.org/10.1371/journal.pone.0006529

Castéra, L., Krieger, S., Rousselin, A., Legros, A., Baumann, J. J., Bruet, O., Brault, B., Fouillet, R., Goardon, N., Letac, O., Baert-Desurmont, S., Tinat, J., Bera, O., Dugast, C., Berthet, P., Polycarpe, F., Layet, V., Hardouin, A., Frébourg, T., & Vaur, D.

(2014). Next-generation sequencing for the diagnosis of heredi-tary breast and ovarian cancer using genomic capture targeting multiple candidate genes. *European Journal of Human Genetics*, *22*(11), 1305–1313. https://doi.org/10.1038/ejhg.2014.16

Chen, V. B., Arendall, W. B., 3rd, Headd, J. J., Keedy, D. A., Immormino, R. M., Kapral, G. J., Murray, L. W., Richardson, J. S., & Richardson, D. C. (2010). MolProbity: All-atom struc-ture validation for macromolecular crystallography. *Acta Crystallographica Section D, Biological Crystallography*, *66*(Pt 1), 12–21. https://doi.org/10.1107/S0907444909042073

Concordet, J. P., & Haeussler, M. (2018). CRISPOR: Intuitive guide selection for CRISPR/Cas9 genome editing experiments and screens. *Nucleic Acids Research*, *46*(W1), W242–W245. https://doi.org/10.1093/nar/gky354

Corbett, K. D., & Berger, J. M. (2003). Structure of the topoisom-erase VI-B subunit: Implications for type II topoisomerase mechanism and evolution. *The EMBO Journal*, *22*(1), 151–163. https://doi.org/10.1093/emboj/cdg008

Corbett, K. D., & Berger, J. M. (2005). Structural dissection of ATP turnover in the prototypical GHL ATPase TopoVI. *Structure*, *13*(6), 873–882. https://doi.org/10.1016/j.str.2005.03.013

D'Arcy, B. M., Blount, J., & Prakash, A. (2019). Biochemical and structural characterization of two variants of uncertain sig-nificance in the PMS2 gene. *Human Mutation*, *40*(4), 458–471. https://doi.org/10.1002/humu.23708

Deschênes, S. M., Tomer, G., Nguyen, M., Erdeniz, N., Juba, N. C., Sepúlveda, N., Pisani, J. E., & Liskay, R. M. (2007). The E705K mutation in hPMS2 exerts recessive, not dominant, effects on mismatch repair. *Cancer Letters*, *249*(2), 148–156. https://doi.org/10.1016/j.canlet.2006.08.008

Dominguez-Valentin, M., Sampson, J. R., Seppälä, T. T., ten Broeke, S., Plazzer, J. P., Nakken, S., Engel, C., Aretz, S., Jenkins, M. A., Sunde, L., Bernstein, I., Capella, G., Balaguer, F., Thomas, H., Evans, D. G., Burn, J., Greenblatt, M., Hovig, E., de Vos tot Nederveen Cappel, W., … Møller, P. (2020). Cancer risks by gene, age, and gender in 6350 carriers of pathogenic mismatch repair variants: Findings from the prospective Lynch syn-drome database. *Genetics in Medicine*, *22*(1), 15–25. https://doi.org/10.1038/s41436-019-0596-9

Drost, M., Koppejan, H., & de Wind, N. (2013). Inactivation of DNA mismatch repair by variants of uncertain significance in the PMS2 gene. *Human Mutation*, *34*(11), 1477–1480. https://doi.org/10.1002/humu.22426

Dutta, R., & Inouye, M. (2000). GHKL, an emergent ATPase/ki-nase superfamily. *Trends in Biochemical Sciences*, *25*(1), 24–28. https://doi.org/10.1016/s0968-0004(99)01503-0

Emsley, P., Lohkamp, B., Scott, W. G., & Cowtan, K. (2010). Features and development of Coot. *Acta Crystallographica Section D, Biological Crystallography*, *66*(Pt 4), 486–501. https://doi.org/10.1107/S0907444910007493

Fishel, R., & Kolodner, R. D. (1995). Identification of mismatch re-pair genes and their role in the development of cancer. *Current Opinion in Genetics & Development*, *5*(3), 382–395. https://doi.org/10.1016/0959-437x(95)80055-7

Geng, H., Du, C., Chen, S., Salerno, V., Manfredi, C., & Hsieh, P. (2011). In vitro studies of DNA mismatch repair pro-teins. *Analytical Biochemistry*, *413*(2), 179–184. https://doi.org/10.1016/j.ab.2011.02.017

Genschel, J., Kadyrova, L. Y., Iyer, R. R., Dahal, B. K., Kadyrov, F. A., & Modrich, P. (2017). Interaction of proliferating cell nuclear antigen with PMS2 is required for MutLalpha activation and function in mismatch repair. *Proceedings of the National Academy of Sciences of the United States of America*, *114*(19), 4930–4935. https://doi.org/10.1073/pnas.1702561114

Guarne, A. (2012). The functions of MutL in mismatch repair: The power of multitasking. *Progress in Molecular Biology and Translational Science*, *110*, 41–70. https://doi.org/10.1016/B978-0-12-387665-2.00003-1

Guarne, A., Junop, M. S., & Yang, W. (2001). Structure and function of the N-terminal 40 kDa fragment of human PMS2: A mono-meric GHL ATPase. *The EMBO Journal*, *20*(19), 5521–5531. https://doi.org/10.1093/emboj/20.19.5521

Hansen, M. F., Johansen, J., Sylvander, A. E., Bjørnevoll, I., Talseth-Palmer, B. A., Lavik, L. A. S., Xavier, A., Engebretsen, L. F., Scott, R. J., Drabløs, F., & Sjursen, W. (2017). Use of multigene-panel identifies pathogenic variants in several CRC-predisposing genes in patients previously tested for Lynch syndrome. *Clinical Genetics*, *92*(4), 405–414. https://doi.org/10.1111/cge.12994

Hinrichsen, I., Weßbecher, I. M., Huhn, M., Passmann, S., Zeuzem, S., Plotz, G., Biondi, R. M., & Brieger, A. (2017). Phosphorylation-dependent signaling controls degradation of DNA mismatch repair protein PMS2. *Molecular Carcinogenesis*, *56*(12), 2663–2668. https://doi.org/10.1002/mc.22709

Hsieh, P., & Yamane, K. (2008). DNA mismatch repair: Molecular mechanism, cancer, and ageing. *Mechanisms of Ageing and Development*, *129*(7–8), 391–407. https://doi.org/10.1016/j.mad.2008.02.012

Huelsman, K. M., Basil, J. B., Sisson, R., Lipe, L. R., Mahon, B., & Draper, D. J. (2021). Somatic tumor profile analysis in a patient with germline PMS2 mutation and synchronous ovarian and uterine carcinomas. *Journal of Personalized Medicine*, *11*(7), 634. https://doi.org/10.3390/jpm11070634

Johnson, J. R., Erdeniz, N., Nguyen, M., Dudley, S., & Liskay, R. M. (2010). Conservation of functional asymmetry in the mamma-lian MutLalpha ATPase. *DNA Repair*, *9*(11), 1209–1213. https://doi.org/10.1016/j.dnarep.2010.08.006

Junop, M. S., Yang, W., Funchain, P., Clendenin, W., & Miller, J. H. (2003). In vitro and in vivo studies of MutS, MutL and MutH mutants: Correlation of mismatch repair and DNA recombina-tion. *DNA Repair*, *2*(4), 387–405. https://doi.org/10.1016/s1568-7864(02)00245-8

Kadyrov, F. A., Dzantiev, L., Constantin, N., & Modrich, P. (2006). Endonucleolytic function of MutLalpha in human mis-match repair. *Cell*, *126*(2), 297–308. https://doi.org/10.1016/j.cell.2006.05.039

Karczewski, K. J., Francioli, L. C., Tiao, G., Cummings, B. B., Alföldi, J., Wang, Q., Collins, R. L., Laricchia, K. M., Ganna, A., Birnbaum, D. P., Gauthier, L. D., Brand, H., Solomonson, M., Watts, N. A., Rhodes, D., Singer-Berk, M., England, E. M., Seaby, E. G., Kosmicki, J. A., … MacArthur, D. (2020). The muta-tional constraint spectrum quantified from variation in 141,456 humans. *Nature*, *581*(7809), 434–443. https://doi.org/10.1038/s41586-020-2308-7

Kolodner, R. (1996). Biochemistry and genetics of eukaryotic mis-match repair. *Genes & Development*, *10*(12), 1433–1442. https://doi.org/10.1101/gad.10.12.1433

Kondo, E., Horii, A., & Fukushige, S. (2001). The interacting domains of three MutL heterodimers in man: hMLH1 interacts with 36 homologous amino acid residues within hMLH3, hPMS1 and

hPMS2. *Nucleic Acids Research*, *29*(8), 1695–1702. https://doi.org/10.1093/nar/29.8.1695

Kosinski, J., Plotz, G., Guarne, A., Bujnicki, J. M., & Friedhoff, P. (2008). The PMS2 subunit of human MutLalpha contains a metal ion binding domain of the iron-dependent repressor protein family. *Journal of Molecular Biology*, *382*(3), 610–627. https://doi.org/10.1016/j.jmb.2008.06.056

Kunkel, T. A., & Erie, D. A. (2015). Eukaryotic mismatch repair in relation to DNA replication. *Annual Review of Genetics*, *49*, 291–313. https://doi.org/10.1146/annurev-genet-112414-054722

Lerner-Ellis, J., Mighton, C., Lazaro, C., Watkins, N., di Gioacchino, V., Wong, A., Chang, M. C., & Charames, G. S. (2021). Multigene panel testing for hereditary breast and ovarian cancer in the province of Ontario. *Journal of Cancer Research and Clinical Oncology*, *147*(3), 871–879. https://doi.org/10.1007/s00432-020-03377-6

Li, G. M. (2008). Mechanisms and functions of DNA mismatch repair. *Cell Research*, *18*(1), 85–98. https://doi.org/10.1038/cr.2007.115

Li, G. M., & Modrich, P. (1995). Restoration of mismatch repair to nuclear extracts of H6 colorectal tumor cells by a heterodimer of human MutL homologs. *Proceedings of the National Academy of Sciences of the United States of America*, *92*(6), 1950–1954. https://doi.org/10.1073/pnas.92.6.1950

Longley, M. J., Pierce, A. J., & Modrich, P. (1997). DNA polymerase delta is required for human mismatch repair in vitro. *The Journal of Biological Chemistry*, *272*(16), 10917–10921. https://doi.org/10.1074/jbc.272.16.10917

Lynch, H. T., Snyder, C. L., Shaw, T. G., Heinen, C. D., & Hitchins, M. P. (2015). Milestones of Lynch syndrome: 1895-2015. *Nature Reviews Cancer*, *15*(3), 181–194. https://doi.org/10.1038/nrc3878

Maxwell, K. N., Hart, S. N., Vijai, J., Schrader, K. A., Slavin, T. P., Thomas, T., Wubbenhorst, B., Ravichandran, V., Moore, R. M., Hu, C., Guidugli, L., Wenz, B., Domchek, S. M., Robson, M. E., Szabo, C., Neuhausen, S. L., Weitzel, J. N., Offit, K., Couch, F. J., & Nathanson, K. L. (2016). Evaluation of ACMG-guideline-based variant classification of cancer susceptibility and non-cancer-associated genes in families affected by breast cancer. *American Journal of Human Genetics*, *98*(5), 801–817. https://doi.org/10.1016/j.ajhg.2016.02.024

Mio, C., Verrienti, A., Pecce, V., Sponziello, M., & Damante, G. (2021). Rare germline variants in DNA repair-related genes are accountable for papillary thyroid cancer susceptibility. *Endocrine*, *73*(3), 648–657. https://doi.org/10.1007/s12020-021-02705-1

Modrich, P., & Lahue, R. (1996). Mismatch repair in replication fidelity, genetic recombination, and cancer biology. *Annual Review of Biochemistry*, *65*, 101–133. https://doi.org/10.1146/annurev.bi.65.070196.000533

Mohd, A. B., Palama, B., Nelson, S. E., Tomer, G., Nguyen, M., Huo, X., & Buermeyer, A. B. (2006). Truncation of the C-terminus of human MLH1 blocks intracellular stabilization of PMS2 and disrupts DNA mismatch repair. *DNA Repair*, *5*(3), 347–361. https://doi.org/10.1016/j.dnarep.2005.11.001

Myler, L. R., Gallardo, I. F., Zhou, Y., Gong, F., Yang, S. H., Wold, M. S., Miller, K. M., Paull, T. T., & Finkelstein, I. J. (2016). Single-molecule imaging reveals the mechanism of Exo1 regulation by single-stranded DNA binding proteins. *Proceedings of the National Academy of Sciences of the United States of America*, *113*(9), E1170–E1179. https://doi.org/10.1073/pnas.1516674113

National Comprehensive Cancer Network. (2021). Genetic/Familial High-Risk Assessment: Colorectal Version 1.2021. https://www.nccn.org/professionals/physician_gls/pdf/genetics_colon.pdf

Nicolaides, N. C., Carter, K. C., Shell, B. K., Papadopoulos, N., Vogelstein, B., & Kinzler, K. W. (1995). Genomic organization of the human PMS2 gene family. *Genomics*, *30*(2), 195–206. https://doi.org/10.1006/geno.1995.9885

Nicolaides, N. C., Littman, S. J., Modrich, P., Kinzler, K. W., & Vogelstein, B. (1998). A naturally occurring hPMS2 mutation can confer a dominant negative mutator phenotype. *Molecular and Cellular Biology*, *18*(3), 1635–1641. https://doi.org/10.1128/MCB.18.3.1635

Papadopoulos, N., Nicolaides, N. C., Wei, Y. F., Ruben, S. M., Carter, K. C., Rosen, C. A., Haseltine, W. A., Fleischmann, R. D., Fraser, C. M., Adams, M. D., Venter, J. C., Hamilton, S. R., Petersen, G. M., Watson, P., Lynch, H. T., Peltomäki, P., Mecklin, J. P., de la Chapelle, A., Kinzler, K. W., & Vogelstein, B. (1994). Mutation of a mutL homolog in hereditary colon cancer. *Science*, *263*(5153), 1625–1629. https://doi.org/10.1126/science.8128251

Peltomaki, P. (2001). Deficient DNA mismatch repair: A common etiologic factor for colon cancer. *Human Molecular Genetics*, *10*(7), 735–740. https://doi.org/10.1093/hmg/10.7.735

Peltomaki, P., & Vasen, H. F. (1997). Mutations predisposing to hereditary nonpolyposis colorectal cancer: Database and results of a collaborative study. The international collaborative group on hereditary nonpolyposis colorectal cancer. *Gastroenterology*, *113*(4), 1146–1158. https://doi.org/10.1053/gast.1997.v113.pm9322509

Perera, S., & Bapat, B. (2008). The MLH1 variants p.Arg265Cys and p.Lys618Ala affect protein stability while p.Leu749Gln affects heterodimer formation. *Human Mutation*, *29*(2), 332. https://doi.org/10.1002/humu.9523

Péron, S., Metin, A., Gardès, P., Alyanakian, M. A., Sheridan, E., Kratz, C. P., Fischer, A., & Durandy, A. (2008). Human PMS2 deficiency is associated with impaired immunoglobulin class switch recombination. *The Journal of Experimental Medicine*, *205*(11), 2465–2472. https://doi.org/10.1084/jem.20080789

Prolla, T. A., Baker, S. M., Harris, A. C., Tsao, J. L., Yao, X., Bronner, C. E., Zheng, B., Gordon, M., Reneker, J., Arnheim, N., Shibata, D., Bradley, A., & Liskay, R. M. (1998). Tumour susceptibility and spontaneous mutation in mice deficient in Mlh1, Pms1 and Pms2 DNA mismatch repair. *Nature Genetics*, *18*(3), 276–279. https://doi.org/10.1038/ng0398-276

Richards, S., Aziz, N., Bale, S., Bick, D., Das, S., Gastier-Foster, J., Grody, W. W., Hegde, M., Lyon, E., Spector, E., Voelkerding, K., Rehm, H. L., & ACMG Laboratory Quality Assurance Committee. (2015). Standards and guidelines for the interpretation of sequence variants: A joint consensus recommendation of the American College of Medical Genetics and Genomics and the Association for Molecular Pathology. *Genetics in Medicine*, *17*(5), 405–424. https://doi.org/10.1038/gim.2015.30

Rossi, B. M., Palmero, E. I., López-Kostner, F., Sarroca, C., Vaccaro, C. A., Spirandelli, F., Ashton-Prolla, P., Rodriguez, Y., de Campos Reis Galvão, H., Reis, R. M., Escremim de Paula, A., Capochin Romagnolo, L. G., Alvarez, K., Della Valle, A., Neffa, F., Kalfayan, P. G., Spirandelli, E., Chialina, S., Gutiérrez Angulo, M., … Dominguez-Valentin, M. (2017). A survey of the clinicopathological and molecular characteristics of patients with

suspected Lynch syndrome in Latin America. *BMC Cancer*, *17*(1), 623. https://doi.org/10.1186/s12885-017-3599-4

Rule, C. S., Patrick, M., & Sandkvist, M. (2016). Measuring in vitro ATPase activity for enzymatic characterization. *Journal of Visualized Experiments*, (114), e54305. https://doi.org/10.3791/54305

Rummel, S. K., Lovejoy, L., Shriver, C. D., & Ellsworth, R. E. (2017). Contribution of germline mutations in cancer predisposition genes to tumor etiology in young women diagnosed with invasive breast cancer. *Breast Cancer Research and Treatment*, *164*(3), 593–601. https://doi.org/10.1007/s10549-017-4291-8

Schofield, M. J., & Hsieh, P. (2003). DNA mismatch repair: Molecular mechanisms and biological function. *Annual Review of Microbiology*, *57*, 579–608. https://doi.org/10.1146/annurev.micro.57.030502.090847

Senter, L., Clendenning, M., Sotamaa, K., Hampel, H., Green, J., Potter, J. D., Lindblom, A., Lagerstedt, K., Thibodeau, S. N., Lindor, N. M., Young, J., Winship, I., Dowty, J. G., White, D. M., Hopper, J. L., Baglietto, L., Jenkins, M. A., & de la Chapelle, A. (2008). The clinical phenotype of Lynch syndrome due to germ-line PMS2 mutations. *Gastroenterology*, *135*(2), 419–428. https://doi.org/10.1053/j.gastro.2008.04.026

Shimodaira, H., Yoshioka-Yamashita, A., Kolodner, R. D., & Wang, J. Y. (2003). Interaction of mismatch repair protein PMS2 and the p53-related transcription factor p73 in apoptosis response to cisplatin. *Proceedings of the National Academy of Sciences of the United States of America*, *100*(5), 2420–2425. https://doi.org/10.1073/pnas.0438031100

Stafford, J. L., Dyson, G., Levin, N. K., Chaudhry, S., Rosati, R., Kalpage, H., Wernette, C., Petrucelli, N., Simon, M. S., & Tainsky, M. A. (2017). Reanalysis of BRCA1/2 negative high risk ovarian cancer patients reveals novel germline risk loci and insights into missing heritability. *PLoS One*, *12*(6), e0178450. https://doi.org/10.1371/journal.pone.0178450

ten Broeke, S., van der Klift, H. M., Tops, C. M. J., Aretz, S., Bernstein, I., Buchanan, D. D., de la Chapelle, A., Capella, G., Clendenning, M., Engel, C., Gallinger, S., Gomez Garcia, E., Figueiredo, J. C., Haile, R., Hampel, H. L., Hopper, J. L., Hoogerbrugge, N., von Knebel Doeberitz, M., le Marchand, L., ... Win, A. K. (2018). Cancer risks for PMS2-associated Lynch syndrome. *Journal of Clinical Oncology*, *36*(29), 2961–2968. https://doi.org/10.1200/JCO.2018.78.4777

Tung, N., Battelli, C., Allen, B., Kaldate, R., Bhatnagar, S., Bowles, K., Timms, K., Garber, J. E., Herold, C., Ellisen, L., Krejdovsky, J., DeLeonardis, K., Sedgwick, K., Soltis, K., Roa, B., Wenstrup, R. J., & Hartman, A. R. (2015). Frequency of mutations in individuals with breast cancer referred for BRCA1 and BRCA2 testing using next-generation sequencing with a 25-gene panel. *Cancer*, *121*(1), 25–33. https://doi.org/10.1002/cncr.29010

van Oers, J. M., Roa, S., Werling, U., Liu, Y., Genschel, J., Hou, H., Jr., Sellers, R. S., Modrich, P., Scharff, M. D., & Edelmann, W. (2010). PMS2 endonuclease activity has distinct biological functions and is essential for genome maintenance. *Proceedings of the National Academy of Sciences of the United States of America*, *107*(30), 13384–13389. https://doi.org/10.1073/pnas.1008589107

Wu, H., Zeng, H., Lam, R., Tempel, W., Kerr, I. D., & Min, J. (2015). Structure of the human MLH1 N-terminus: Implications for predisposition to Lynch syndrome. *Acta Crystallographica Section F: Structural Biology Communications*, *71*(Pt 8), 981–985. https://doi.org/10.1107/S2053230X15010183

Yurgelun, M. B., Kulke, M. H., Fuchs, C. S., Allen, B. A., Uno, H., Hornick, J. L., Ukaegbu, C. I., Brais, L. K., McNamara, P., Mayer, R. J., Schrag, D., Meyerhardt, J. A., Ng, K., Kidd, J., Singh, N., Hartman, A. R., Wenstrup, R. J., & Syngal, S. (2017). Cancer susceptibility gene mutations in individuals with colorectal cancer. *Journal of Clinical Oncology*, *35*(10), 1086–1095. https://doi.org/10.1200/JCO.2016.71.0012

SUPPORTING INFORMATION

Additional supporting information may be found in the online version of the article at the publisher's website.